TURUN YLIOPISTON JULKAISUJA
ANNALES UNIVERSITATIS TURKUENSIS

SARJA - SER. A I OSA - TOM. 447

ASTRONOMICA - CHEMICA - PHYSICA - MATHEMATICA

ENVIRONMENTS OF ACTIVE GALAXIES

by

Heidi Lietzen

TURUN YLIOPISTO
UNIVERSITY OF TURKU
Turku 2012

From the Department of Physics and Astronomy
University of Turku
Turku, Finland

Supervised by

Dr. Pekka Heinämäki and Dr. Pasi Nurmi
Tuorla Observatory, Department of Physics and Astronomy
University of Turku
Turku, Finland

Reviewed by

Dr. Peter Johansson
Department of Physics
University of Helsinki
Helsinki, Finland

and

Prof. Volker Müller
Leibniz-Institut für Astrophysik
Potsdam (AIP)
Potsdam, Germany

Opponent

Prof. Arthur Chernin
Sternberg Institute
Moscow University
Moscow, Russia

ISBN 978-951-29-5171-0 (PRINT)
ISBN 978-951-29-5172-7 (PDF)
ISSN 0082-7002
Painosalama Oy - Turku, Finland 2012

It was six men of Indostan
To learning much inclined,
Who went to see the Elephant
(Though all of them were blind),
That each by observation
Might satisfy his mind.

The Blind Men and the Elephant by John Godfrey Saxe

Acknowledgments

Working on this thesis has been a wonderful experience. I have enjoyed both, the regular day-to-day work, and the special moments in conferences, summer schools, and parties. It has been a great pleasure to meet all the nice people in Tuorla and around the world. I want to thank you all for helping me with this inspiring work.

Most importantly, I want to thank my supervisors, Pekka Heinämäki and Pasi Nurmi. They have always given me all the support and advise I have needed, and I have truly enjoyed the long discussions about the details of the papers. I have been extremely lucky for getting the possibility to be part of such a good research group. I also want to thank Leo Takalo for his help, advise and support in getting funding, finding papers to read, and writing the papers for this thesis.

I also want to thank the rest of our research group: our collaborators at Tartu Observatory. The contribution of Jaan Einasto, Maret Einasto, Mirt Gramann, Juhan Liivamägi, Enn Saar, Erik Tago, and Elmo Tempel has been important for the papers in this thesis. I could not have done this research without their help.

The work in this thesis has been financially supported by Emil Aaltonen Foundation, Finnish Cultural Foundation, Magnus Ehrnrooth's Foundation, Turku University Foundation, and the Academy of Finland. I also thank people who helped me get the funding by writing recommendation letters and giving suggestions for improving my research plans.

I want to thank all the people working at Tuorla Observatory for the great working environment. I thank the people who made my days happy with funny discussions at the coffee table. I thank Sarah Bird, Auni Somero, and Tommi Vornanen for sharing the office and the good and the difficult moments of thesis work. I thank people who worked with me at Tuorla Planetarium for the pleasant experiences in educating and entertaining the general public.

Finally, I want to thank my family, and most importantly, my husband, Toni Lyytikäinen for their love and support.

Heidi Lietzen

Abstract

This dissertation presents studies on the environments of active galaxies.

Paper I is a case study of a cluster of galaxies containing BL Lac object RGB 1745+398. We measured the velocity dispersion, mass, and richness of the cluster. This was one of the most thorough studies of the environments of a BL Lac object. Methods used in the paper could be used in the future for studying other clusters as well.

In Paper II we studied the environments of nearby quasars in the Sloan Digital Sky Survey (SDSS). We found that quasars have less neighboring galaxies than luminous inactive galaxies. In the large-scale structure, quasars are usually located at the edges of superclusters or even in void regions. We concluded that these low-redshift quasars may have become active only recently because the galaxies in low-density environments evolve later to the phase where quasar activity can be triggered.

In Paper III we extended the analysis of Paper II to other types of AGN besides quasars. We found that different types of AGN have different large-scale environments. Radio galaxies are more concentrated in superclusters, while quasars and Seyfert galaxies prefer low-density environments. Different environments indicate that AGN have different roles in galaxy evolution. Our results suggest that activity of galaxies may depend on their environment on the large scale.

Our results in Paper III raised questions of the cause of the environment-dependency in the evolution of galaxies. Because high-density large-scale environments contain richer groups and clusters than the underdense environments, our results could reflect smaller-scale effects. In Paper IV we addressed this problem by studying the group and supercluster scale environments of galaxies together. We compared the galaxy populations in groups of different richnesses in different large-scale environments. We found that the large-scale environment affects the galaxies independently of the group richness. Galaxies in low-density environments on the large scale are more likely to be star-forming than those in superclusters even if they are in groups with the same richness.

Based on these studies, the conclusion of this dissertation is that the large-scale environment affects the evolution of galaxies. This may be caused by different “speed” of galaxy evolution in low and high-density environments: galaxies in dense environments reach certain phases of evolution earlier than galaxies in underdense environments. As a result, the low-density regions at low redshifts are populated by galaxies in earlier phases of evolution than galaxies in high-density regions.

Contents

List of publications

I *Clustering environment of BL Lacertae object RGB 1745+398*
Lietzen, H., Nilsson, K., Takalo, L. O., Heinämäki, P., Nurmi, P., Keinänen, P., and Wagner, S.
A&A **482**, 771 (2008)

II *Environments of nearby quasars in Sloan Digital Sky Survey*
Lietzen, H., Heinämäki, P., Nurmi, P., Tago, E., Saar, E., Liivamägi, L. J., Tempel, E., Einasto, M., Einasto, J., Gramann, M., and Takalo, L. O.
A&A **501**, 145 (2009)

III *Large scale environments of z<0.4 AGN*
Lietzen, H., Heinämäki, P., Nurmi, P., Liivamägi, L. J., Saar, E., Tago, E. Takalo, L. O., Einasto, M.
A&A **535**, A21 (2011)

IV *Environments of galaxies in groups within the supercluster-void network*
Lietzen, H., Tempel, E., Heinämäki, P., Nurmi, P., Einasto, M., and Saar, E.
A&A **545**, A104 (2012)

CHAPTER 1
Introduction

Research on galaxy evolution has advanced greatly in recent years. Main reason of this increase of knowledge comes from the new deep and wide galaxy surveys and space missions. Surveys have revealed a three-dimensional web-like structure of the universe. The general observed properties of the universe seem to be in accordance with the predictions of the concordance cosmological model. Although there is a statistical agreement between theory and observations, many details of the non-linear evolution of galaxies are not well understood. These issues include the dichotomy of galaxies in the blue cloud and red sequence, the relation between the masses of the bulge of a galaxy and the supermassive black hole in its center, and the regulation of growth of massive galaxies. This thesis presents a study on low-redshift galaxies from the point of view of their environment, concentrating especially on active galaxies. The goal of this thesis is to study the connection between the activity in galaxies and their large-scale environment.

One aspect that has recently been found important is the role of active galactic nuclei (AGN) in galaxy evolution. Simulations of galaxies with semi-analytical models of evolutionary processes have lead to a theory, where the feedback from the active supermassive black hole in the center of a galaxy affects the evolution. Theories suggest two types of AGN feedback, which are often called the quasar mode and the radio mode. Quasar mode is responsible for expelling gas from galaxies, and thus quenching star formation. Radio mode feedback regulates the growth of massive galaxies by heating the gas.

Galaxies do not evolve isolated. Instead, they are members of groups and clusters of galaxies, and on the large scale, they form superclusters and filaments, with empty voids between them. Evolution of galaxies is tied to the evolution of the whole universe. Structures are assembled through gravitational collapse of dark matter, and galaxies form when baryonic matter gathers to the centers of dark matter halos through complex gas-dynamical processes, most importantly through radiative cooling of gas. Halos merge and structures grow more massive. Galaxies interact with each others during their evolution. As the result, we have the galaxies we observe at low redshifts: star-forming spiral and passive elliptical galaxies, with different types of activity in their nuclei: quasars, Seyfert galaxies, radio galaxies, and BL Lacertae objects.

Environment in which the galaxies are located plays an important role in galaxy evolution. Observations have shown that galaxy populations in dense environments are different from those in low-density regions (Dressler 1980; Postman & Geller 1984; Hamilton 1988; Gómez et al. 2003; Kauffmann et al. 2004). Different environments also provide different dynamics between galaxies: velocity dispersions vary from 100 km s^{-1}

of small groups to 1500 $\mathrm{km\,s^{-1}}$ of the richest clusters (Bahcall 1981). Finally, simulations have shown that galaxy evolution and thus properties depend on the assembly history of the dark matter halo in which the galaxy resides. Gao et al. (2005) showed that halos that assemble early are much more clustered than halos of the same mass that assemble late.

Evolution of galaxies, their activity, and the large-scale environment is an extensive field. This thesis will give a short summary on the background observational and theoretical results important in this field. The following three chapters will cover the observational information on galaxies (Chapter 2), the large-scale structures (Chapter 3), and AGN (Chapter 4). They will be followed by two chapters on the theory of structure formation in Chapter 5 and galaxy evolution in Chapter 6.

CHAPTER 2
Galaxies

The First approach'd the Elephant,
And happening to fall
Against his broad and sturdy side,
At once began to bawl:
"God bless me! but the Elephant
Is very like a wall!"

The Blind Men and the Elephant by John Godfrey Saxe

2.1 Classification of galaxies

Galaxies are the basic building blocks of the Universe. Their cosmological significance has been clear since the 1920s, when Edwin Hubble confirmed that some of the observed nebulae were truly objects outside the Milky Way. Hubble found that galaxies have various shapes and sizes, and that they move away from the observer, their speed increasing with the distance (Hubble 1926, 1927).

Galaxies can be divided in classes based on their morphology. The basic morphology classes can be described with the Hubble's sequence, a tuning-fork diagram shown in Fig. 2.1. The basic classes are elliptical, lenticular, spiral, and irregular galaxies. Spiral galaxies can be further divided into regular and barred spirals. Elliptical and spiral galaxies are often called early and late-type galaxies respectively. These names refer to their places in the Hubble's sequence, where the ellipticals are plotted to the left, not to their ages or other evolutionary aspects.

Besides morphology, galaxies can be divided in two distinct classes by their colors (Gavazzi et al. 2010). Color is connected to the morphology: elliptical galaxies are nearly always red, while spiral galaxies are mostly blue. A color-magnitude diagram of galaxies is shown in Fig. 2.2. It shows how the galaxy population is divided in two classes: the blue cloud and the red sequence. The blue cloud consists of spiral galaxies, while the red sequence contains mostly ellipticals. Between the blue cloud and the red sequence the galaxy population forms a 'green valley', where the number of galaxies is lower. The distribution of galaxies seen in Fig. 2.2 also shows that the most luminous galaxies are typically red.

The classification of galaxies into different morphological types has traditionally been done by visual inspection. A successful example of a classification of a large sample of galaxies is the Galaxy Zoo project (Lintott et al. 2008). A problem with visual classification is always the subjectivity of the classifier and, especially at high redshifts,

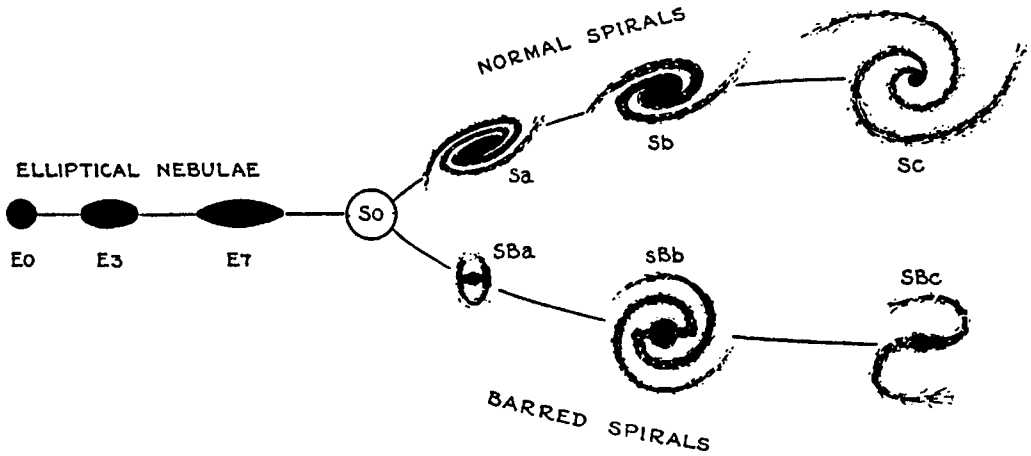

Figure 2.1: *Hubble's sequence of galaxies. Figure from Hubble (1936).*

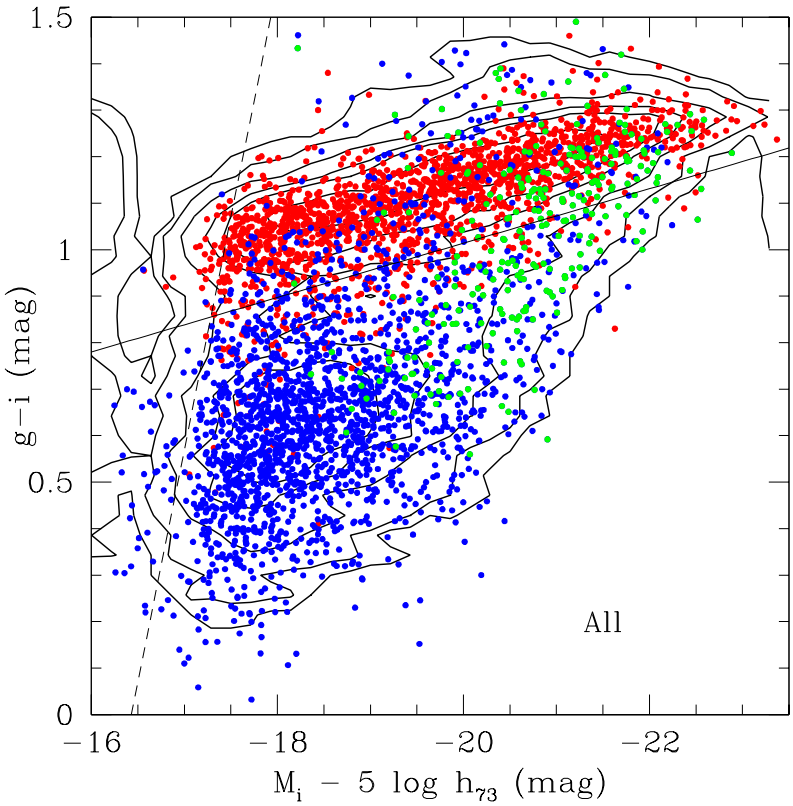

Figure 2.2: *Color-magnitude diagram of galaxies in the Coma Supercluster. Galaxies are coded according to their morphology, so that the red points refer to elliptical or lenticular galaxies, blue points to disk-dominated spiral galaxies, and the green points to bulge-dominated spiral galaxies. Figure from Gavazzi et al. (2010).*

the fact that all galaxies do not fit clearly in any of the classes. Furthermore, as the visual classification requires vast amount of work, automatic classification criteria have also been used. These classification criteria are based on different observed properties of galaxies of different types. For example, Huertas-Company et al. (2011) used three parameters to classify galaxies: light concentration, axis ratio, and color.

2.2 Morphology

Spiral galaxies typically consist of a thin disk with spiral arms, a central bulge, and often a bar. Some spiral galaxies are more disk-dominated (Sc type on the right-hand side of the Hubble diagram), while others are more bulge-dominated (Sa type). The relative significance of the disk and the bulge can be studied by measuring the surface-brightness profile of the galaxy. The surface brightness profile describes the stellar density distribution, which is more central-concentrated in bulge-dominated galaxies. The surface-brightness profile of a galaxy can be described with a Sérsic profile

$$I(r) = I_e \exp\left[-\beta_n \left(\left(\frac{r}{r_e}\right)^{1/n} - 1\right)\right], \tag{2.1}$$

where β_n is chosen so that r_e, the effective radius, includes half of the light, and $I_e = I(r_e)$. The Sérsic index n determines the curvature of the profile (Sersic 1968). The surface brightness profile of a disk typically has a Sérsic index $n = 1$, which is an exponential profile, while the bulge has a Sérsic index $n = 4$, known as the de Vaucouleurs profile (de Vaucouleurs 1948). The profile of a spiral galaxy is usually a combination of these two. According to Blanton et al. (2003), the Sérsic index of a galaxy is strongly correlated with the color: the blue galaxies have typically nearly exponential profiles, while redder galaxies are more concentrated. This is a crude simplification though, naturally all the components of a galaxy affect the total brightness profile.

As Fig. 2.2 shows, the spiral galaxies have mostly blue colors. The bulge-dominated spirals are redder than the disk-dominated. However, as Driver et al. (2006) points out, the galaxy population does not consist of two classes but two components, red bulges and blue disks. Color is related to star-formation rate of a galaxy: young stars are bluer than old ones, making galaxies with a high star-formation rate blue.

Elliptical galaxies have an apparently simple structure of a smooth, elliptical surface brightness distribution. They are shown with the red points in the color-magnitude diagram in Fig. 2.2, which shows that they are redder than most spiral galaxies, and that they include the most luminous galaxies. While the surface brightness profile of spiral galaxies is a combination of a disk and a bulge, elliptical galaxies have no sign of a disk. According to Driver et al. (2006), a typical Sérsic index for elliptical galaxies is $n = 4$, similarly to the bulge-dominated spiral galaxies. Elliptical galaxies are close to true ellipses, but there are small deviations from the simple axisymmetric form. The elliptical galaxies can be divided into two subclasses: disky, with peaked isophotes, and boxy,

with box-shaped isophotes (Bender 1988). Kormendy et al. (2009) showed that disky elliptical galaxies typically have low Sersic indices, $n \simeq 3 \pm 1$, while boxy ellipticals have very large Sersic indices, $n > 4$.

2.3 Star formation

Stars form in dense molecular clouds (see Williams et al. 2000, for a review). Because of that, star-formation activity of a galaxy can be estimated by its gas content. The relation between star-formation density Σ_{SFR} and gas density Σ_{gas} can be described by the empirical Kennicutt-Schmidt law, which was first formulated by Schmidt (1959). In its basic form, the law can be written as

$$\Sigma_{\mathrm{SFR}} = A\Sigma_{\mathrm{gas}}^{N}, \tag{2.2}$$

where A and N are constants. This empirical law suggests that the star-formation rate may be controlled by the self-gravity of gas.

Strongly star-forming galaxies can be recognized spectroscopically by their emission-line ratios. Baldwin et al. (1981) introduced the BPT (Baldwin, Phillips & Terlevich) diagram, where galaxies with emission lines can be divided in star-forming galaxies and AGNs based on two emission-line ratios. A BPT diagram by Brinchmann et al. (2004) is shown in Fig. 2.3. The differences in line ratios between star-forming galaxies and AGNs are caused by different photoionization mechanisms causing the emission: hot stars in star-forming galaxies, and non-thermal continuum or fast shocks in AGNs. In AGNs the level of ionization and temperature are higher than in H II regions generated by young massive stars. Thus the AGN is surrounded by a larger partially ionized zone. This causes a rise of emission lines such as the forbidden line [N II], which is nearly absent in galaxies photoionized by OB stars.

Elliptical galaxies usually have red colors, which are associated with old stars. Therefore, red color is a sign of a low star-formation rate. There are some exceptions though: based on an analysis on emission lines using the BPT diagram, Fukugita et al. (2004) found that approximately 3 % of early-type galaxies are star-forming.

Star-formation rate of galaxies evolves with redshift. At $z > 1$, high-luminosity galaxies experience rapid star formation. According to Madau et al. (1998), global star-formation rate reaches its peak value at redshift $z \approx 1.5$. At lower redshifts the luminosity of star-forming galaxies declines smoothly until the present epoch (Cowie et al. 1996).

2.4 Galaxy dynamics

The stars and gas in the disk of a spiral galaxy move in the disk plane on almost circular orbits. This movement can be described with a rotation curve. As a function of radius,

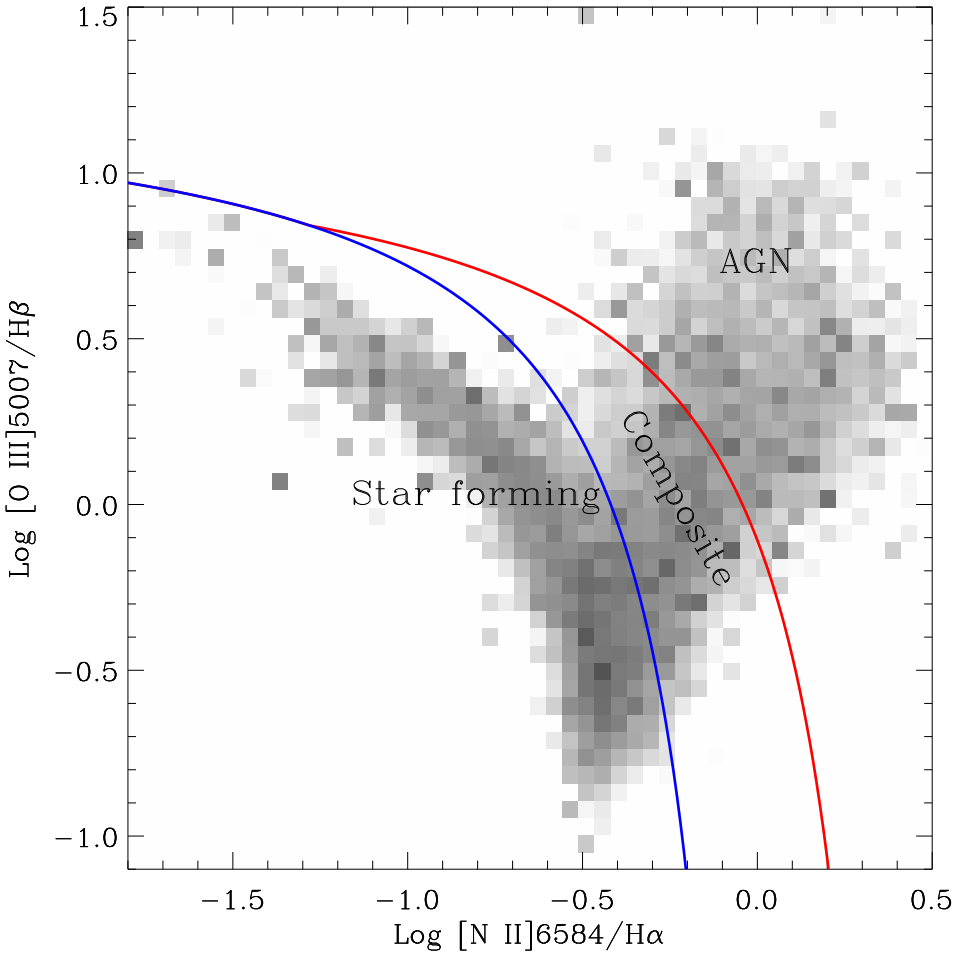

Figure 2.3: *The distribution of emission-line galaxies in the BPT diagram. Figure from Brinchmann et al. (2004)*

the rotation curves stay flat instead of declining, while visible light declines exponentially. This is one of the signs of the existence of dark matter. The scaled rotation curves show that the shape of the curves is similar regardless of the surface brightness of the galaxy, suggesting a "universal rotation curve" (Persic et al. 1996; Swaters et al. 2000).

Luminosity of the disk is connected to the rotational velocity of a galaxy through the empirical Tully-Fisher relation (Tully & Fisher 1977). The relation shows a tight correlation between the maximum of the rotation curve and the total luminosity of a galaxy. The correlation shows that even though only a small fraction of the mass of a galaxy is luminous, the luminosity is still related to the total mass.

Elliptical galaxies do not rotate in the way the spiral galaxies do. Instead, the stars

move in the galaxy in random motion. The dynamics of an elliptical galaxy can be described by its velocity dispersion σ. Mass in a virialized system can be determined using the velocity dispersion and the virial radius of a galaxy:

$$M \approx \frac{\sigma^2 R_{vir}}{G}. \tag{2.3}$$

Velocity dispersion of elliptical galaxies is related to luminosity through the Faber-Jackson relation (Faber & Jackson 1976) similarly to the Tully-Fisher relation in spiral galaxies. The B band luminosity depends on the velocity dispersion by the relation $L_B \propto \sigma^4$ (Faber & Jackson 1976). The relation between the rotational velocity and the velocity dispersion (v/σ) is typically in the range from 0.1 to 1 for elliptical galaxies, and from 10 to 20 for spiral galaxies (Davies et al. 1983; Vega Beltrán et al. 2001).

Ferrarese & Merritt (2000) found that central velocity dispersion of a galaxy is tightly correlated with the mass of the central black hole. Their best-fit relation between the central stellar velocity dispersion σ_c and the black-hole mass M_{bh} was

$$\log M_{\mathrm{bh}} = 4.80(\pm 0.55) \log \sigma_c - 2.9(\pm 1.3), \tag{2.4}$$

where M_{bh} is in units of solar mass and σ_c in kilometers per second. This relation holds for both, elliptical and spiral galaxies. This relation suggests that the evolution of the black hole and its host galaxy may be connected. The most prominent sign of the supermassive black holes are the different types of AGN, and the finding of the M–σ relation has strengthened the role of AGN in galaxy evolution.

CHAPTER 3
Large scale structure

The Second, feeling of the tusk,
Cried, -"Ho! what have we here
So very round and smooth and sharp?
To me 'tis mighty clear
This wonder of an Elephant
Is very like a spear!"

The Blind Men and the Elephant by John Godfrey Saxe

3.1 Groups and clusters of galaxies

The characteristic scale of the first acoustic peak at $\theta \simeq 1^\circ$in the cosmic microwave background (CMB) spectrum indicates the maximum scale of the causally connected acoustic (baryon-photon sound waves) oscillations at the time of recombination. This degree scale fluctuation corresponds to a co-moving scale of 100 h^{-1}Mpc in the Universe today. At scales larger than this the galaxy distribution turns homogeneous. On smaller scales, galaxies are not distributed in space randomly. Instead they form coherent structures. While there are apparently isolated galaxies as well, most galaxies belong to a group or a cluster of galaxies. A group of galaxies typically contains less than $\sim$50 galaxies, and richer systems are called clusters. However, there is no clear and exact definition of the limit between a group and a cluster. Individual clusters contain more galaxies than smaller groups, but the groups are more numerous. Therefore more galaxies in total are found in groups — there are more galaxies, where there are less galaxies.

Groups and clusters of galaxies are assumed to be virialized systems of galaxies although this is a simplified assumption. While the virial conditions apply to bound systems, systems of galaxies are not always bound, and therefore not virialized. Niemi et al. (2007) concluded that approximately 20 % of nearby groups of galaxies are not bound systems. The galaxies in a group or a cluster are also assumed to share a common dark matter halo. Groups of galaxies are held together by the mutual gravitational attraction between the galaxies and the dark matter. In clusters, the velocities of galaxies are higher than in groups, and therefore, they must contain more dark matter to hold the cluster together (Bahcall 1981). Clusters also contain more hot gas than groups.

A basic characteristic of a group or a cluster is its richness, the number of its galaxies. Determining richness of a group or a cluster is difficult because of various sources

of uncertainty. The main problems when using photometric observations are contamination from foreground and background galaxies, the difficulty of observing faint galaxies and the uncertainty in the redshifts of galaxies. Several methods have been created to describe the richness of a cluster. The first comprehensive catalog of clusters of galaxies was published by Abell (1958). Based on this study, the richness of a cluster is still often expressed by Abell richness class. The richness class is based on the number of galaxies in the cluster that are not more than two magnitudes fainter than the third brightest member of the cluster. Richness class 0 cluster contains from 30 to 49 galaxies, class 1 from 50 to 79 galaxies, class 2 from 80 to 129 galaxies, class 3 from 130 to 199 galaxies, class 4 from 200 to 299 galaxies, and class 5 more than 299 galaxies.

The cluster-center galaxy correlation amplitude $B_{\rm gc}$ is a much used measure for cluster richness especially in studies on the cluster-scale environments of active galaxies. The method was first used by Longair & Seldner (1979) to study the environments of radio galaxies. $B_{\rm gc}$ takes into account the number of background and foreground galaxies and normalizes the galaxy counts using a known luminosity function. These corrections increase the robustness of the $B_{\rm gc}$ as a measure for richness. It is relatively insensitive to magnitude limit, areal coverage, and photometric errors.

To determine $B_{\rm gc}$, the number of galaxies is first calculated inside an appropriate radius around the center. A usual radius is 500 kpc, which corresponds to a typical size of a cluster. The number of background galaxies is then counted on an field of the same surface area near the cluster. With these numbers, the angular cross-correlation function is

$$A_{\rm gc} = \frac{N_{\rm tot} - N_{\rm b}}{N_{\rm b}} \frac{3-\gamma}{2} \theta^{\gamma-1}, \tag{3.1}$$

where $N_{\rm tot}$ is the number of galaxies within the circle radius, $N_{\rm b}$ is the number of background galaxies, θ is the circle radius in angular units, and γ is the slope of the correlation function, usually assumed to be 1.77. The angular correlation function is then scaled with the universal luminosity function $\Phi(m_{\rm lim}, z)$ to get

$$B_{\rm gc} = \frac{N_{\rm g} A_{\rm gc}}{\Phi(m_{\rm lim}, z) I_\gamma} d^{\gamma-3}. \tag{3.2}$$

Here I_γ is an integration constant, d is the distance of the cluster, and $N_{\rm g}$ is the average surface density of galaxies. Typical values for clusters with Abell richness class 0–5 are $B_{\rm gc} = (600 \pm 200)$ Mpc$^{1.77}$, $B_{\rm gc} = (1000 \pm 200)Mpc^{1.77}$, $B_{\rm gc} = (1400 \pm 200)Mpc^{1.77}$, $B_{\rm gc} = (1800 \pm 200)Mpc^{1.77}$, $B_{\rm gc} = (2200 \pm 200)Mpc^{1.77}$, and $B_{\rm gc} = (2400 \pm 200)Mpc^{1.77}$, respectively (Yee & López-Cruz 1999). This method has often been used for estimating clustering around different types of AGN. In that case the AGN is taken as the center, and galaxies are counted in a circle surrounding it. This was one of the methods used in Paper I.

Velocity dispersion of groups and clusters vary from $\sim$100 km s^{-1} of small groups to $\sim$1500 km s^{-1} of rich clusters. Velocity dispersion is strongly correlated to richness:

$$N_{0.5}^c = 21 (v_r / 1000 {\rm km\,s^{-1}})^{1.2}, \tag{3.3}$$

where v_r is the radial velocity dispersion, and $N^c_{0.5}$ is the number of galaxies in a circle of 0.5 Mpc (Bahcall 1981).

The most important characteristic determining the properties of clusters of galaxies is their mass. The mass of a cluster can be determined using several techniques, such as galaxy kinematics, X-ray profiles, or gravitational lensing. Typical mass of a cluster (M_{500}, mass of the region in which the density is more than 500 times the mean density) is between 10^{14} and $10^{15} M_\odot$. Mass is tightly correlated with the optical luminosity of a cluster (Popesso et al. 2005). Mass-to-light ratio depends on mass: for the poor groups with mass of 10^{12} to $10^{13} M_\odot$, mass-to-light ratio is approximately $100h(M_\odot/L_\odot)_B$, while for clusters of $10^{15} M_\odot$, the ratio may be $500h(M_\odot/L_\odot)_B$ (Parker et al. 2005).

While optical observations see the individual galaxies in groups and clusters, X-rays can be used for studying a group or a cluster as a whole. X-ray emission from a cluster of galaxies was first found in the Coma cluster by Gursky et al. (1971). They suggested that the source of X-ray radiation may be the hot intergalactic gas in the cluster. This idea was supported by Bahcall (1977), who found that X-ray luminosity is correlated with the richness of the cluster. However, this correlation does not hold in small groups, possibly because mergers of galaxies are more frequent in small groups, causing variation in group richness (Ponman et al. 1996). Since the intracluster gas follows the gravitational potential of the cluster, X-rays can be used as a reliable measure for cluster mass.

3.2 Supercluster scale

Groups and clusters of galaxies are distributed in a web-like large-scale structure. Similar structures can be produced theoretically using the linear perturbation theory and the Zel'dovich approximation, where the particles move on straight-line trajectories until the first non-linear structures, the so-called Zel'dovich pancakes form. Regions with high density of groups and clusters form superclusters, which are connected by filaments. Between these structures, there are voids with low galaxy density with diameters even as large as $\sim$100 Mpc (Jõeveer & Einasto 1978). The supercluster-void network represents the density distribution of the very early universe: dense regions in the early density fluctuations have evolved to regions of high galaxy density. Figure 3.1 gives an example of two superclusters. Groups of galaxies are marked with circles with sizes proportional to group richness.

The large-scale cell structure can be studied using large galaxy surveys, such as the two degree Field Galaxy Redshift Survey (2dF; Colless et al. (2001); Percival et al. (2001)), the Two Micron All Sky Survey (2MASS; Skrutskie et al. (2006)), and Sloan Digital Sky Survey (SDSS; York et al. (2000); Stoughton et al. (2002), Aihara et al. (2011)).

Due to the unvirialized nature of superclusters, a luminosity-density field is an appropriate method of finding and identifying superclusters. In clusters, mass is tightly connected to the total optical luminosity. Because of that, luminosity can be used to

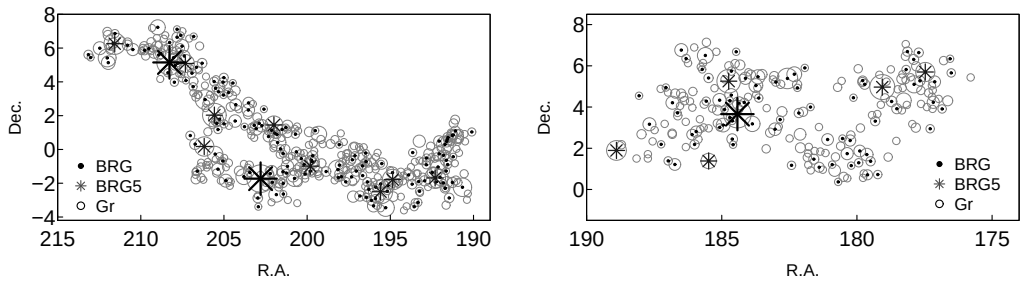

Figure 3.1: *Groups of galaxies in two rich superclusters in the Sloan Great Wall. Circles represent groups of galaxies with symbol sizes proportional to the richness of the group. Dots mark groups that host up to four bright red galaxies, and stars represent groups with five or more bright red galaxies. Figure from Einasto et al. (2011)*

trace the mass of the structures. The density field was first used by Davis & Huchra (1982) to calculate the gravitational field in the nearby universe.

Einasto et al. (2003) present the method of determining the luminosity-density field. The field is based on a galaxy catalog with distance and absolute magnitude known for each galaxy. Coordinates of galaxies are transformed into rectangular coordinates for minimizing projection effects. The density field is then smoothed with an appropriate smoothing scale to see the structures of that scale. In Papers II, III, and IV, we used the luminosity-density field to determine the large-scale environments of different types of galaxies and AGN.

Every galaxy is assumed to be a member of a density enhancement, such as a group or a cluster. Part of the galaxies in these groups and clusters fall outside the observed magnitude window. This has to be corrected by using a weight factor W_L. The weight can be determined as the ratio of the expected total luminosity to the expected luminosity in the visibility window:

$$W_L = \frac{\int_0^\infty L\phi(L)\mathrm{d}L}{\int_{L_1}^{L_2} L\phi(L)\mathrm{d}L}. \tag{3.4}$$

Galaxy luminosities can be assumed to be distributed according to the Schechter (1976) function

$$\phi(L)\mathrm{d}L \propto (L/L^*)^\alpha \exp(-L/L^*)\mathrm{d}(L/L^*), \tag{3.5}$$

where α and L^* are constants. The total luminosity is then

$$L_{\mathrm{tot}} = L_{\mathrm{obs}} W_L, \tag{3.6}$$

where $L_{\mathrm{obs}} = L_\odot 10^{0.4\times(M_\odot - M)}$ is the luminosity of the galaxy with absolute magnitude M.

After correcting the luminosities with the weight factor, the luminosity-density field with corrected luminosities can be calculated in a Cartesian grid. Cell size in the grid can be chosen to fit the data. A denser grid gives a higher resolution if needed, but

causes challenges for computing power and disk space if the field is large in volume. For studying superclusters, the grid size is typically 1 Mpc.

The field is then smoothed to an appropriate scale to show the structures of the correct size. A smoothing length of 1 to 2 h^{-1} Mpc will produce a density field that shows clusters of galaxies. For superclusters, the field is often smoothed on scales of 8 h^{-1} Mpc (Einasto et al. 2007b).

Figure 3.2 shows a luminosity density field based on a catalog of luminous red galaxies (LRGs) in the SDSS. In this field the grid cell size is 3 h^{-1} Mpc and the smoothing length is 16 h^{-1} Mpc. LRGs can be used instead of all galaxies because they are usually concentrated in the centers of clusters. This makes them good indicators of clusters and the high-density regions of the large-scale structures (Gladders & Yee 2000). Because LRGs are the most luminous galaxies, they can be observed at larger distances. This makes it possible to construct a density field with larger volume. In Paper III we used the luminosity-density field of the LRGs to study the large-scale environments of different types of AGN. The large volume of the LRG sample made it possible to study the environments of over 8 000 AGNs in total.

Superclusters are conventionally defined as regions with density above a certain threshold. For example, Tempel et al. (2009) used a threshold of 4.6 times the mean density of the field as a minimum density level of superclusters. Their definition of voids was a density of less than 1.5 times the mean density. As a new approach Liivamägi et al. (2012) took into account the richness difference of superclusters by using an adaptive threshold. Generally, the supercluster threshold is chosen to be approximately the percolation density, which is the level where the individual superclusters start to be separated from each other.

Superclusters vary in size, richness, and shape. They may form a single filament, a branching system of filaments, or a diffuse cloud of clusters (Einasto et al. 2003). Rich supercluster are less symmetrical than poor ones, and the mean density grows with the total luminosity of a supercluster (Einasto et al. 2007a).

The Local Group of galaxies belongs to the Local Supercluster, which is also known as the Virgo Supercluster. The Local Supercluster is a typical poor supercluster. Its total luminosity is $L \approx 3 \times 10^{12} h^{-2} L_{\odot}$ and its mass is $M \approx 10^{15} h^{-1} M_{\odot}$ (Einasto et al. 2007d). The richest and largest supercluster known so far is the Sloan Great Wall (SGW) (Gott et al. 2005). The total luminosity of the SGW is $4 \times 10^{13} h^{-2} L_{\odot}$. Einasto et al. (2011) found that the SGW can be divided into several individual superclusters that have had different formation histories and evolutions. Two examples of these superclusters are shown in Fig. 3.1. Because of this, the SGW may not be a genuine physical structure but an assembly of many rich superclusters.

Superclusters and filaments surround void areas with very low galaxy densities. Voids are roughly spheroidal with a typical semi-major axis of $\sim$20 h^{-1} Mpc (Plionis & Basilakos 2002). Voids are extremely underdense. According to Hoyle & Vogeley (2004), their average density contrast is $\delta\rho/\rho = -0.9$, where density contrast $\delta\rho/\rho = -1$ refers to zero density of galaxies. The galaxies they contain are usually

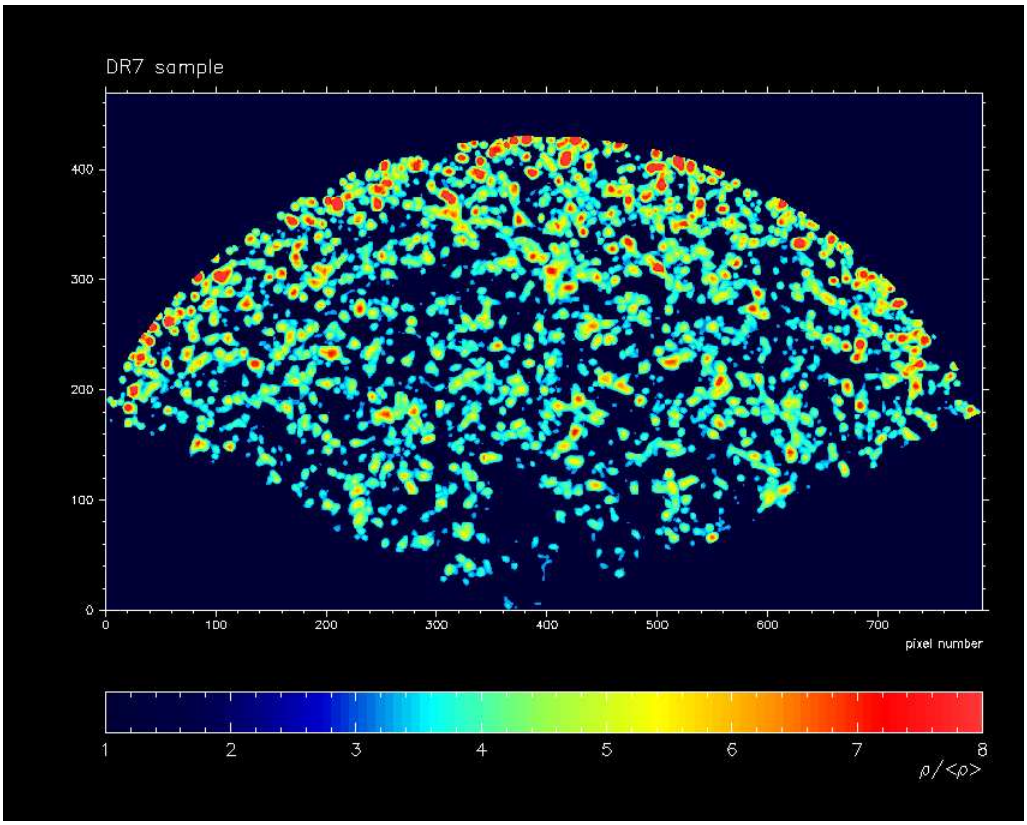

Figure 3.2: *Luminosity density field of LRGs. Colors represent different density levels: blue areas are voids, while the red areas are the densest cores of superclusters. The coordinates show the grid cell numbers, with one grid cell corresponding $3h^{-1}$ Mpc. Originally published in Paper III.*

located close to the edges. Total volume of voids is approximately 40 % of the volume of the local universe.

3.3 Galaxy populations in different environments

Different group or cluster-scale environments have different galaxy populations. This was first discovered as the morphology-density relation (Dressler 1980; Postman & Geller 1984). Regions with high galaxy density are populated mostly by elliptical galaxies, while in the less dense environments spiral galaxies dominate. Similarly, the local density is correlated with star-formation rate and luminosity. Galaxies in high-density environments are more luminous than those in underdense regions (Hamilton 1988). Strongly star-forming galaxies are located in lower density environments than galaxies with little star formation (Gómez et al. 2003). This is expected, as the star-formation rate

and morphology are connected as was discussed in Chapter 2. However, environment affects the star-formation rate even when the morphology is the same. Spiral galaxies with red color, and therefore low star-formation rate, are located in higher density environments than bluer spiral galaxies (Bamford et al. 2009). Star formation depends more strongly on the environment than morphology (Kauffmann et al. 2004; Blanton et al. 2005).

Butcher & Oemler (1978) found that clusters at redshift $z \sim 0.4$ contain considerably more blue galaxies than nearby similar clusters. This redshift-dependency has become known as the Butcher-Oemler effect. Besides the larger fraction of spirals, Couch et al. (1994) found that galaxies at these intermediate redshift also show more signs of interaction than galaxies in nearby clusters. Dressler et al. (1999) also found spectral features typical to poststarburst galaxies in the redshift range of $z = 0.37 - 0.56$. These results indicate that galaxies in clusters are evolving with redshift.

A dependency between the properties of galaxies and their environment can also be seen on the supercluster scale. The morphology-density relation on the large scale was first detected by Einasto & Einasto (1987). Skibba et al. (2009) found that the color of galaxies depends strongly on environment on all scales from 0.1 to $10h^{-1}$ Mpc. They detected the color-environment relation both in spiral and elliptical galaxies, but no correlation between the morphology and environment when the color was fixed. In filaments connecting two rich clusters, Porter et al. (2008) found that the star-formation rate of galaxies increases with the distance from the clusters. Star formation peaks at 2–3 h^{-1} Mpc from the clusters, suggesting that at this distance the gas of the cluster may start to affect the galaxies.

The galaxy populations are also different in rich and poor superclusters: rich superclusters contain a higher fraction of passive, red, early-type galaxies than poor superclusters. In the densest cores of rich superclusters there is an excess of red galaxies in groups with equal richness and even among isolated galaxies that do not belong in a group (Einasto et al. 2007c, 2008). According to Tempel et al. (2011), the luminosity function of elliptical galaxies depends strongly on the large-scale environment. These results suggest that both the local environment (group or cluster) and the supercluster-scale environment may affect galaxy morphology and their star-formation activity. The question of effects on different scales on star-forming activity of galaxies is discussed in Paper IV. We found indications that the large-scale environment may affect the star-forming activity in galaxies independently of the richness of the group in which the galaxy resides.

CHAPTER 4
Active galactic nuclei

The Third approached the animal,
And happening to take
The squirming trunk within his hands,
Thus boldly up and spake:
"I see," quoth he, "the Elephant
Is very like a snake!"

The Blind Men and the Elephant by John Godfrey Saxe

Active galactic nuclei (AGNs) are the most luminous objects in the Universe. Their luminosity comes from the central region of a galaxy, and the most probable engine of the activity is the supermassive black hole in the center of the host galaxy. The observed AGNs can be divided into several classes: quasars, Seyfert galaxies, radio galaxies, and BL Lacertae objects. On a more general level, AGNs can be classified as radio-loud and radio-quiet AGNs.

The systematic study of AGNs was started by Carl Seyfert, who detected emission lines in spectra of six galaxies (Seyfert 1943). This type of radio-quiet, low-luminosity AGN was later named Seyfert galaxies. Finding other types of AGN was linked to the advances in radio astronomy. First radio sources were found by Reber (1944), and Bolton et al. (1949) achieved the first optical identification of radio sources. A number of radio sources were found in the third Cambridge survey (3C; Edge et al. 1959), and many radio-loud AGNs are therefore known by their 3C numbers.

While some of the 3C radio sources could be associated with galaxies, others were optically point sources. These point-sources with peculiar emission lines in their optical spectra were named quasi-stellar sources or quasars. The spectral emission lines proved that these sources were at high redshift (Schmidt 1963; Greenstein 1963). This finding was the beginning of quasar research.

The last type of AGN found was the BL Lacertae (BL Lac) objects. Schmitt (1968) identified the “variable star” BL Lacertae with the radio source VRO 42.22.01. Strittmatter et al. (1972) found that BL Lac and four other objects were similar to quasars, except for the fact that they had no spectral emission lines.

4.1 Different types

4.1.1 Seyfert galaxies

Seyfert galaxies are the least luminous type of AGN. They have the morphology of a normal spiral galaxy, but have emission lines in their spectra. Their typical luminosities are in the range of $-23 < M_V < -20$. They are classified as radio-quiet AGNs, but some of them emit weakly in the radio regime, with a power of $P_{1.4\,\mathrm{GHz}} < 10^{23.5}\,\mathrm{W\,Hz^{-1}}$. In the nearby universe Seyfert galaxies are the most common type of AGN.

Seyfert galaxies can be divided in two subclasses based on the width of their emission lines. Seyfert 1 galaxies have broad emission lines with full-width half maxima of more than $1\,000\,\mathrm{km\,s^{-1}}$, while Seyfert 2 type galaxies have only narrow emission lines (Khachikian & Weedman 1974). Emission lines often found in Seyfert galaxies include Hα, Hβ, and forbidden lines [O III], and [N II]. Intensity-ratios of these lines can also be used to distinguish between AGNs and star-forming galaxies as was discussed in section 2. Besides the pure Seyfert 1 and 2 galaxies, there are also galaxies with composite spectra, which are often marked by labels such as Seyfert 1.8 and 1.9 (Osterbrock 1981).

4.1.2 Quasars

Quasars belong to the most luminous objects in the Universe with optical magnitude $M_V < -23$. They can be divided in two subclasses, radio-quiet and radio-loud quasars. Approximately 10 % of quasars are radio loud (Kellermann et al. 1989). The limiting radio power between radio-quiet and radio-loud quasars is usually defined at $P_{1.4\,\mathrm{GHz}} = 10^{25}\,\mathrm{W\,Hz^{-1}}$. Radio-loud quasars can further be divided into two classes based on the shape of their radio continuum. The spectrum is usually described by a power law with $S \propto \nu^{\alpha_r}$, where S is the radio power, ν is frequency, and α_r is the slope of the spectrum. Steep-spectrum radio quasars have a spectrum with a slope $|\alpha_r| > 0.5$, while the slope of flat-spectrum quasars is $|\alpha_r| < 0.5$ (Urry & Padovani 1995). Morphology of radio sources is connected to the steepness of the spectrum: steep-spectrum sources are more compact than those with a flat spectrum.

Quasars have broad emission lines in their spectra, similarly to Seyfert 1 galaxies. The higher luminosity is the only characteristic separating radio-quiet quasars from the Seyfert 1 galaxies.

Quasars are relatively common: the SDSS Data Release 7 quasar catalog (Schneider et al. 2010) contains 105 783 spectroscopically confirmed quasars. Due to their high luminosity, quasars can be detected at greater distances, with redshifts even as high as $z = 7.1$ (Mortlock et al. 2011). The peak in quasar space-density is at redshift $z \approx 2$ (Maloney & Petrosian 1999). Star-formation peaks nearly at the same epoch ($z \sim 1.5$; Madau et al. 1998), indicating a connection between quasar activity and star-formation.

Host galaxies of quasars are difficult to study because the luminous nucleus dominates over the galaxy. According to a study of 15 radio-quiet quasars by Hyvönen et al.

(2007b), the host galaxies of quasars in the redshift range $0.5 < z < 1$ are luminous elliptical galaxies. Host galaxies of radio-quiet quasars are $\sim$0.5 magnitudes fainter than those of radio-loud quasars.

4.1.3 Radio galaxies

Radio galaxies are characterized by extended radio emission lobes that can reach to even scales of a few Mpc. Optically radio galaxies are giant elliptical galaxies. Fanaroff & Riley (1974) classified radio galaxies into two types based on the morphology of their radio emission. FR I radio galaxies have their highest radio emission near the nucleus, while in FR II radio galaxies the luminosity peaks at the edges of their lobes.

FR II galaxies have a higher radio luminosity than FR I galaxies. An approximate division between the two types can be made with radio power $P_{1.4\,\mathrm{GHz}} = 10^{25}\,\mathrm{W\,Hz^{-1}}$. However, this is not an exclusive limit: there are more luminous radio galaxies with FR I morphology and less luminous FR II galaxies as well. The host galaxies of FR II galaxies are usually more luminous than those of FR I, but there is no strong correlation between the radio and optical luminosities (Ledlow & Owen 1996).

High-luminosity radio galaxies usually have optical spectra with strong emission lines similar to Seyfert galaxies. In low-luminosity radio galaxies the emission lines are often missing (Hine & Longair 1979). These low-excitation radio galaxies (LERGs) also lack X-ray emission, which is typically observed in other types of AGNs (Hardcastle et al. 2006). These characteristics hint that LERGs may be fueled differently from other AGNs.

According to Snellen & Best (2001) the local space density of FR I radio galaxies is 170 per Gpc^3. FR II type galaxies are considerably rarer. At higher redshifts radio galaxies are difficult to find. Snellen & Best (2001) found two FR I radio galaxies at $z > 1$ in the Hubble Deep Field, which covers 10×10 arcmin^2 area of sky. This result suggests that their density at high redshift is higher than at low redshifts. This implies evolution in the radio galaxy abundance. By comparing the radio luminosity function of radio galaxies in the redshift range $0.4 < z < 0.7$ to the radio luminosity function of local population, Sadler et al. (2007) also found clear evidence of cosmic evolution in low-power radio galaxies.

4.1.4 BL Lac objects

BL Lac objects are characterized by a nearly featureless optical spectrum, high radio and X-ray luminosity, strong polarization, and high variability (Kollgaard 1994). With the exception of featureless spectrum, these properties are also typical of optical violently variable (OVV) quasars. Therefore BL Lac objects and OVVs are often grouped together as a class of blazars (Angel & Stockman 1980).

All BL Lac objects are radio loud (Stocke et al. 1990). Their radio structure is dominated by a luminous core, surrounded by only faint extended emission (Perlman

& Stocke 1994). Besides radio, BL Lac objects are also strong X-ray emitters. Most BL Lac objects have been found through either radio or X-ray surveys. Finding BL Lac objects through optical surveys is difficult. The lack of spectral lines makes especially the determination of redshifts difficult. Partly because of the difficulties in finding them, partly because they are unusual, the number of known BL Lac objects is smaller than the number of other types of AGN.

Nilsson et al. (2003) studied the host galaxies of 100 BL Lac objects. They found that the host galaxies of BL Lac objects are elliptical galaxies with average magnitudes of $M_R = -23.9 \pm 0.8$. They are similar to radio galaxies and normal ellipticals.

4.2 Structure and unification

Although the different types of AGN are observed with different properties, it is generally believed that their fueling mechanisms are essentially similar. The foundations of a unified scheme between the different types of AGN were put together in review articles by Antonucci (1993) and Urry & Padovani (1995). Antonucci (1993) defined a preliminary simple model of two basic types of AGN: radio quiet and radio loud. Seyfert galaxies and radio-quiet quasars belong to the radio-quiet group, while radio galaxies, radio-loud quasars, and BL Lac objects make the radio-loud group. Urry & Padovani (1995) further divided the radio-loud subclass in two intrinsically different types based on their radio luminosity: the high-luminosity sources, such as radio-loud quasars and FR II radio galaxies, and the low-luminosity sources, such as BL Lac objects and FR I radio galaxies. With this division, all AGNs belong in one of three physically different types. Differences between AGN in each of these types are caused by different viewing angles from which we observe them.

The structure of an AGN is illustrated in Fig. 4.1. The source of energy is the gravitational potential energy of the supermassive black hole in the center. The black hole is surrounded by a luminous accretion disk. Above the accretion disk there are gas clouds that move rapidly and thus cause the broad-line emission. The disk is surrounded by a thick dusty torus that obscures the broad-line region if the AGN is viewed side-ways. The gas clouds farther from the disk move more slowly and produce the narrow emission lines. Finally, outflows of energetic particles form collimated jets that are observed as radio lobes.

The strength and morphology of the radio jet is the main difference between the three separate AGN types. Radio-quiet AGNs have an extremely weak jet or no jet at all, and the radio-loud AGNs can be divided in two classes based on the strength of the jet. Wilson & Colbert (1995) suggested that the formation of a jet may depend on the spin of the black hole. The jet is also connected to the host galaxy: Seyfert galaxies with no jet are spiral galaxies, while radio galaxies are ellipticals.

According to the unified scheme, the differences between the different types of AGNs within a radio-luminosity based class are caused by orientation of the viewing

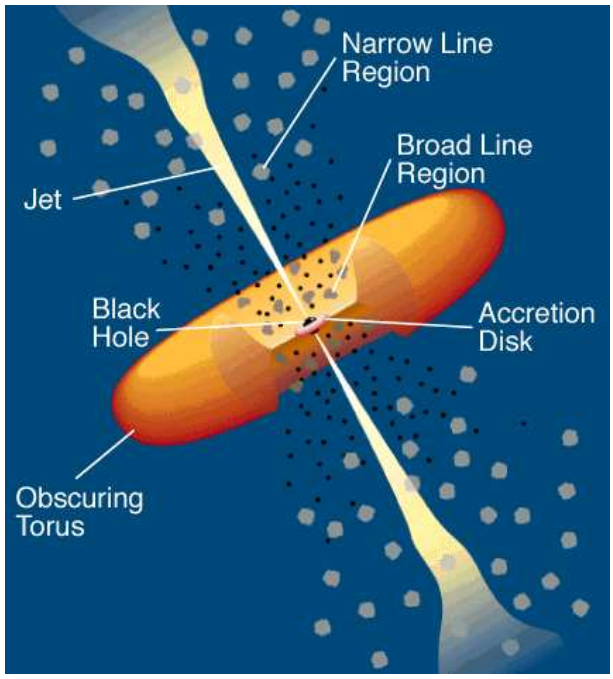

Figure 4.1: *The basic structure of a radio-loud AGN from Urry & Padovani (1995). The sizes of the components are not to scale.*

angle. Seyfert 2 galaxies are viewed 'edge on', so that the torus blocks the broad-line regions from our view. Seyfert 1 galaxies and radio-quiet quasars are viewed more 'face on', so that the broad-line regions are visible. The difference between Seyfert 1 galaxies and quasars is the luminosity: quasars are basically very luminous Seyfert 1 galaxies. Because of this, a class of 'quasar 2', an obscured quasar analogous to Seyfert 2 is expected to exist. They are difficult to find, but some candidates have been detected using a selection based on mid-infrared color (Hickox et al. 2007).

The radio-loud unification schemes are based on orientation of the jet. AGNs viewed perpendicular to the jet are radio galaxies. When the jet is weak, they usually have FR I type morphology, and when the jet is stronger, their morphology is usually characteristic to the FR II class. When a radio galaxy is viewed from the direction of the jet, it should be observed as a BL Lac object if the jets are weak, or a radio-loud quasar when the jets are strong.

A summary of properties of the main types of AGN and their assumed viewing angles are shown in Table 4.1. Since it is not possible to turn an AGN around and see what it looks like from another viewing angle, proving the unified schemes is based on indirect evidence. A test for unification is to study properties of AGN that are independent of orientation. These properties should be the same for physically similar objects.

One property that should be independent of orientation is the narrow-line emission. As Fig. 4.1 presents, the narrow-line regions extend to distances that cannot be obscured

Table 4.1: *Summary of AGN characteristics. Typical radio powers (column 2) were adapted from Woltjer (1990).*

Type	$P_{1.4\mathrm{GHZ}}$ [W Hz^{-1}]	Host galaxy	Viewing angle
Radio-quiet quasar	$< 10^{25}$	elliptical	face on
Seyfert 1	$< 10^{23}$	spiral	face on
Seyfert 2	$< 10^{23}$	spiral	edge on
FR I	$10^{23.5} \ldots 10^{25}$	elliptical	perpendicular to the jet
BL Lac	$> 10^{23.5}$	elliptical	parallel to the jet
FR II	$> 10^{25}$	elliptical	perpendicular to the jet
Radio-loud quasar	$> 10^{25}$	elliptical	parallel to the jet

by torus and thus hidden from view. Studies by Jackson & Browne (1990) and Hes et al. (1993) support the unification scheme: they found that different types of AGN have similar narrow-line emission.

Host galaxies of AGNs are often used for testing the unification model. Their properties do not depend on the orientation of the nucleus, and therefore they should be similar between physically similar AGNs with different orientation. Hyvönen et al. (2007a) studied a sample of 18 BL Lac host galaxies and compared their colors to those of 19 quasars by Jahnke et al. (2004) and 50 radio galaxies by Govoni et al. (2000). They found that the host galaxies of BL Lac objects are similar to those of quasars and radio galaxies: elliptical galaxies with slightly bluer colors than passive elliptical galaxies. This result is not in conflict with the unification model. On the other hand, Best & Heckman (2012) found that high-excitation radio galaxies are hosted by lower-mass galaxies than low-excitation radio galaxies. This supports the idea that the weakly radio-loud AGNs are intrinsically different from the high-luminosity radio sources.

4.3 Environments of AGNs

The first results on the environments of AGNs were from Bahcall et al. (1969), who showed that five quasars were associated with clusters of galaxies. Later several studies on the nearby environments of different types of AGN have been made using the spatial galaxy-galaxy cross-correlation amplitude B_{gg} (Longair & Seldner 1979). The method was presented in detail in Sect. 3.1

De Robertis et al. (1998) found that the mean B_{gg} for Seyfert 1 galaxies is $\langle B_{\mathrm{gg}} \rangle = 28.7$ Mpc$^{1.77}$, and for Seyfert 2 galaxies 45.4 Mpc$^{1.77}$. The result for Seyfert 2 galaxies was close to their control sample of nonactive galaxies, while Seyfert 1 galaxies were less clustered. The difference in the environments of Seyfert 1 and Seyfert 2 galaxies was also found by Dultzin-Hacyan et al. (1999). They suggest that the difference could be explained by interaction with the neighboring galaxies which could drive more

molecular gas toward the center of the galaxy, and thus increasing obscuration.

Environments of quasars have been studied by Yee & Green (1984), Ellingson et al. (1991), Fisher et al. (1996), and Wold et al. (2000). A typical environment for quasars is a small group of galaxies, although some of them may also be found in richer clusters. Radio-loud quasars tend to have higher clustering in their environment than the radio quiet quasars. Wold et al. (2000) found a mean $\langle B_{\rm gg} \rangle = 107$ Mpc$^{1.77}$ for radio-quiet quasars and $\langle B_{\rm gg} \rangle = 365$ Mpc$^{1.77}$ for radio-loud quasars. They suggest that this difference may be due to more efficient fueling for quasars in rich environments, causing triggering of radio-loud quasars only in rich environments.

Radio galaxies are found in high-density environments. McLure & Dunlop (2001) found an average of $\langle B_{\rm gg} \rangle = 575$ Mpc$^{1.77}$. According to Hill & Lilly (1991), the environments of radio galaxies depend on their radio power and redshift. They found that the redshift dependency is stronger for FR II type galaxies than for those with FR I type morphology. At redshift $z \sim 0$, FR I radio galaxies are found in slightly richer environments than the FR II. Because sources with higher power can be detected from a larger distance, the differences caused by redshift cannot be separated from differences caused by power.

According to Wurtz et al. (1997), a typical environment of BL Lac objects is a poor cluster. Their average cross-correlation amplitude is $\langle B_{\rm gg} \rangle = 209$ Mpc$^{1.77}$. RGB 1745+398, which we studied in Paper I, is one of the BL Lacs in richer environments, having $B_{\rm gg} \approx 600$ Mpc$^{1.77}$.

Large-scale environments of AGNs provide for a test of the unification model. The orientation of the nucleus does not depend on the group of galaxies, or even large-scale environment in which its host galaxy resides. The environmental studies have provided evidence against the unification model. BL Lac objects have local environments more typical to FR II type radio galaxies and radio-loud quasars than to FR I radio galaxies. This suggests that FR I galaxies may not be the parent population of BL Lac objects as the unified scheme predicts. Kharb et al. (2010) also detected characteristics more typical to FR II radio galaxies in the radio emission of some BL Lac objects. These findings included extended luminosities and hot spots that are often found in radio-loud quasars. Based on these findings, it is possible that BL Lac objects may not constitute a homogeneous population that fits in the simple unified scheme. Instead, BL Lac objects may have both, FR I and FR II galaxies as their parent population.

More recently the large galaxy surveys have made more extensive studies on AGN environments possible. Li et al. (2006) analyzed the clustering of $\sim$90 000 narrow-line AGN. They found that on scales larger than a few Mpc, these AGNs are clustered similarly to the inactive control sample. On scales between 100 kpc and 1 Mpc, AGNs are clustered more weakly than the control galaxies. Coldwell & Lambas (2006) studied the environments of $\sim$2 000 $z < 0.2$ quasars in the SDSS. They found that quasars avoid dense regions. They also found that galaxies close to quasars (at distance of less than 1 Mpc) were bluer and had higher star-formation rates than galaxies in similar environments without a nearby quasar. In Paper II we also found the underdensity in

the environments of quasars. Quasars have less neighboring galaxies on scales of a few Mpc than luminous nonactive galaxies. On the large scale, they are usually located at the edges of superclusters.

With the increase of data, comparisons between the environments of different types of AGNs have become easier. A large number of each type can be studied together to find if their environments are the same or not. Donoso et al. (2010) studied the environments of 14 000 radio-loud AGNs, including radio galaxies and quasars. They calculated cross-correlation functions between the AGNs and LRGs, and found that radio AGNs are clustered more strongly than quasars, including both, radio-loud and radio-quiet quasars. The difference between radio galaxies and radio-loud quasars suggests that these types are likely to be triggered by different physical mechanisms.

Differences between the environments of different types of AGN are partly connected to the types of AGN host galaxies: hosts of radio galaxies are red elliptical galaxies in dense environments, while Seyfert galaxies are spiral galaxies in lower densities. According to Hickox et al. (2009), radio and X-ray selected AGNs are clustered similarly to their host galaxy populations, but infrared-selected AGNs are weakly clustered relative to a matched galaxy sample. These findings suggest that different types of AGN are likely to be triggered in different environments. We found this difference between the environment of different types of AGN on the large scale in Paper III. Based on the luminosity-density field we found that a typical environment for Seyfert galaxies and quasars is a void or a low-density filament. Radio galaxies are more likely to be in superclusters. BL Lac objects are also often in high-density environments, but their fraction in void environments is higher than that of radio galaxies.

Table 4.2: *Small and large-scale environments of AGNs. Small-scale environments are expressed with the average B_{gg} value. Due to different assumptions in different studies, the values may not be fully comparable. The large-scale environments are shown as the average density of the luminosity-density field in the environment of each type as found in Paper III. References for B_{gg} values: (a) Wold et al. (2000), (b) De Robertis et al. (1998), (c) McLure & Dunlop (2001), (d) Wurtz et al. (1997).*

Type	$\langle B_{\rm gg} \rangle$ [Mpc$^{1.77}$]	$\langle D \rangle$
Radio-quiet quasars	$107^{(a)}$	1.71
Seyfert 1 galaxies	$29^{(b)}$	1.73
Seyfert 2 galaxies	$45^{(b)}$	1.65
Radio galaxies	$575^{(c)}$	3.01
BL Lac objects	$209^{(d)}$	2.5
Radio-loud quasars	$365^{(a)}$	1.8

Table 4.2 summarizes the small and large-scale environments of different types of AGN. The small-scale environments are shown as the average galaxy-galaxy cross-correlation amplitude $B_{\rm gg}$ found by Wurtz et al. (1997) for BL Lac objects, De Robertis

et al. (1998) for Seyfert galaxies, Wold et al. (2000) for quasars, and McLure & Dunlop (2001) for radio galaxies. Since these studies have been based on slightly different assumptions e.g. on the cosmological parameters, and study different redshift ranges ($z < 1$ in all cases though), the results are comparable only on a qualitative level. The large-scale environments are given as average densities of the luminosity-density field in Paper III. The values are in units of the mean density of the whole field.

As Table 4.2 shows, on both scales radio-quiet quasars and Seyfert galaxies are found in low-density environments, while radio galaxies and BL Lac objects are located in richer regions. For radio-loud quasars the local environment is rich, but the large-scale density quite low. When interpreting results on radio-loud quasars, one must remember that they are rare objects. The study by Wold et al. (2000) is based on 21 radio-loud quasars, and the result on the large scale in Paper III on 26. This reduces the reliability of the results because of random variation. A more reliable study of radio-loud quasars is the one by Donoso et al. (2010), who had a sample of 307 radio-loud quasars. Their result shows clearly that there is no significant difference in clustering strength between radio-loud and radio quiet quasars, and both types are less clustered than radio galaxies.

CHAPTER 5
Structure formation

The Fourth reached out his eager hand,
And felt about the knee.
"What most this wondrous beast is like
Is mighty plain," quoth he,
"'Tis clear enough the Elephant
Is very like a tree!"

The Blind Men and the Elephant by John Godfrey Saxe

5.1 Cosmological background

Currently the most popular theories for structure formation are based on the Λ cold dark matter (ΛCDM) cosmology. Λ refers to the cosmological constant, the vacuum energy of space, or dark energy. It was first introduced by Einstein (1917) to keep the cosmology model static. When the Universe was found to be expanding, the cosmological constant was not needed anymore. It was taken back to the models after Riess et al. (1998) and Perlmutter et al. (1999) found using type Ia supernovae that the expansion of the Universe is speeding up.

The standard cosmology starts with the assumption of cosmological principle that the universe is homogeneous and isotropic at sufficiently large scales. Under this assumption the geometry of the four-dimensional space-time leads to the Robertson-Walker form of the space-time metric

$$\mathrm{d}s^2 = \mathrm{d}t^2 - a^2(t)\left[\mathrm{d}r^2/(1-kr^2) + r^2\mathrm{d}\theta^2 + r^2\sin^2\theta\mathrm{d}\phi^2\right], \tag{5.1}$$

where r, θ, and ϕ are the co-moving spatial coordinates and t is time. The expansion is described by the cosmic scale factor $a(t)$, and k is the curvature of three-dimensional space: -1 for negative, 0 for flat, or 1 for positive curvature.

Redshift of light emitted at time t_{em} can be defined as $z = \lambda_{obs}/\lambda_{em} - 1 = 1/a(t_{em}) - 1$. Time is related to the redshift by $\mathrm{d}t = -\mathrm{d}z/H(z)(1+z)$, where $H = \dot{a}/a$ is the Hubble parameter.

The connection between the geometry and the physical content of the universe is given by the Einstein equations. Together with Robertson-Walker metric (Eq. 5.1), Einsteins equations lead to the Friedmann equations

$$H^2 = \frac{8\pi G\rho}{3} - \frac{k}{a^2} + \frac{\Lambda}{3}, \tag{5.2}$$

and

$$\frac{\ddot{a}}{a} = -\frac{4\pi G}{3}(\rho + 3P) + \frac{\Lambda}{3}, \tag{5.3}$$

where ρ is the total density of the Universe and P is the total pressure.

Time dependency of pressure and density fluctuations in adiabatic processes can be described by the fluid equation

$$\dot{\epsilon} + 3H\left(\epsilon + \frac{P}{c^2}\right) = 0, \tag{5.4}$$

where ϵ is the energy density and P is the pressure. If we assume that $P = w\epsilon$, where w is a constant, the fluid equation has a solution

$$\frac{\epsilon}{\epsilon_0} = \left(\frac{a}{a_0}\right)^{-3(1+w)}. \tag{5.5}$$

This solution gives the energy density as a function of a. The radiation pressure of photons derived from blackbody radiation distribution is $P = \rho c^2/3$. Therefore, for a universe with only radiation, $w = 1/3$ and $\epsilon \propto a^{-4}$. Non-relativistic matter can be approximated pressureless, making $w = 0$ and $\epsilon \propto a^{-3}$. If the universe is dominated by vacuum energy (Λ), $w = -1$, which keeps the energy density constant. In reality, all these components work together, but the evolution can be approximated by using the dominant component only. In the beginning, radiation dominates until the matter-radiation equality at redshift $z \sim 3233$, after which matter becomes dominant. At recombination ($z \sim 1100$) the radiation can escape from the matter, and the radiation of this epoch is seen as the cosmic microwave background. The latest phase of the evolution of the universe is the domination of the vacuum energy, which starts at redshift $z \sim 0.85$.

If $k = 0$, density ρ is the critical density

$$\rho_c = \frac{3H^2}{8\pi G}. \tag{5.6}$$

Using the critical density, the matter density parameter can be defined as

$$\Omega_m = \frac{\rho}{\rho_c} = \frac{8\pi G\rho}{3H^2}. \tag{5.7}$$

This includes both, dark matter and baryonic matter. Similarly we can define the density parameter Ω_Λ for the vacuum energy:

$$\Omega_\Lambda = \frac{8\pi G\rho_\Lambda}{3H^2} = \frac{\Lambda c^2}{3H^2}. \tag{5.8}$$

The total density parameter consists of the different components of energy: $\Omega = \Omega_\Lambda + \Omega_m$. The density parameter determines the geometry of the Universe. If $\Omega < 1$, the

Universe is negatively curved or open, if $\Omega = 1$, the Universe is flat, and if $\Omega > 1$, the Universe is positively curved or a closed universe.

The density parameters can be determined with a combination of observational results. Supernova Ia's tell us that the expansion of the universe is accelerating, providing evidence for the Λ term (Riess et al. 1998; Perlmutter et al. 1999). Based on mass-to-light ratios of clusters of galaxies, Bahcall et al. (1995) suggested that the matter density parameter Ω_m is between 0.2 and 0.3. From the results of Wilkinson Microwave Anisotropy Probe (WMAP) (Jarosik et al. 2011) we know that the biggest temperature differences in the cosmic microwave background (CMB) are separated by approximately 1°. This implies that the universe is flat.

These observations together lead to the current ΛCDM concordance cosmology model, where the value of the total density parameter is $\Omega = 1.080^{+0.093}_{-0.071}$, the dark energy density $\Omega_\Lambda = 0.734 \pm 0.029$, and the matter density $\Omega_m = 0.258 \pm 0.030$ (Jarosik et al. 2011).

The CMB radiation is very uniform on the large scale (more than 1°). Currently the temperature of the CMB corresponds to 2.725 K black body radiation spectrum (Mather et al. 1999). On smaller scales, however, the CMB is characterized by tiny fluctuations of 10^{-5} K (Smoot et al. 1992). The anisotropic structure of the CMB was formed at the epoch of recombination, at redshift ($z \sim 1100$). Before the recombination, photons were constantly scattered because of the presence of the free electrons through Thomson scattering. At the recombination, protons and electrons started to form neutral hydrogen, letting the previously bound photons move freely. The baryonic matter, which had previously been oscillating with the photons, could now start to follow the structure growth of dark matter.

The observed anisotropy of the CMB gives a picture of the initial density perturbations. Figure 5.1 shows the foreground-reduced internal linear combination map based on the five year WMAP data (Hinshaw et al. 2009). The density fluctuations can be seen on different colors in the Figure. These density fluctuations provide seeds for structure growth.

5.2 Initial structure formation

According to the current ΛCDM model the density fluctuations seen in the CMB are the seeds of the formation of structure of the Universe. The small fluctuations can grow due to gravitational instability, and finally collapse into the first stars and galaxies. In the 'bottom up' scheme of galaxy and cluster formation, small structures are formed first and later they gather together to form larger structures. In the early universe, where the perturbations are small, the linear perturbation theory describes the structure formation. Perturbations are adiabatic, and therefore they affect the number densities of matter and radiation similarly.

In the early Universe, the growth of the density perturbations is linear. The cos-

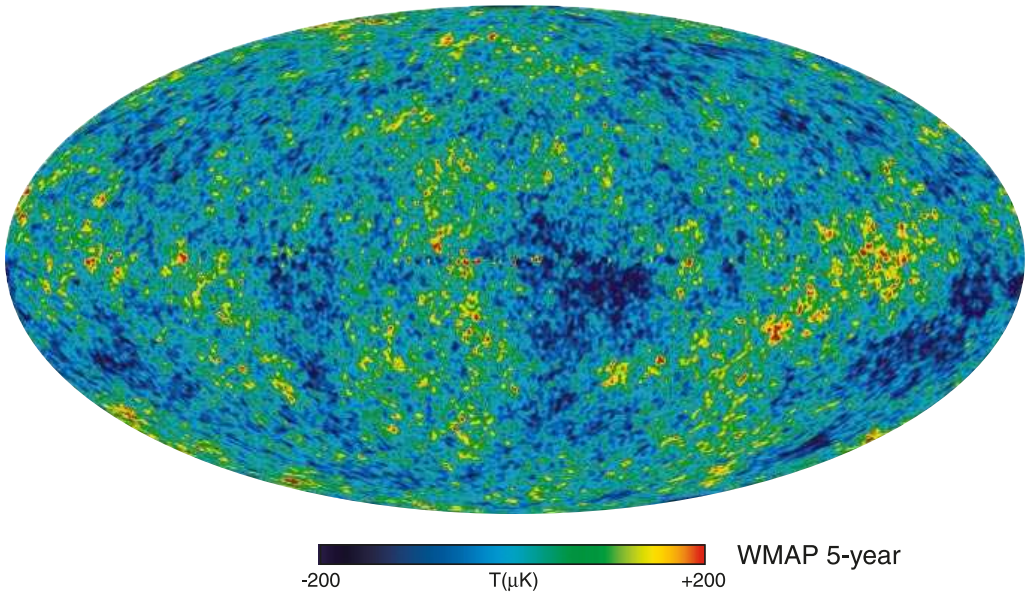

Figure 5.1: *The foreground-reduced Internal Linear Combination (ILC) map based on the five year WMAP data. Image from Hinshaw et al. (2009).*

mological expansion can be described assuming that the cold dark matter is an ideal pressure-less fluid, with baryonic matter having a pressure P (Barkana & Loeb 2001; Mo et al. 2010). The relative density perturbation at a co-moving position $\mathbf{x}$ is

$$\delta(\mathbf{x}) = \frac{\rho(\mathbf{r})}{\bar{\rho}} - 1, \tag{5.9}$$

where $\mathbf{r}$ is the fixed coordinate that corresponds to $\mathbf{x}$, and $\bar{\rho}$ is the mean density. Linear theory is valid while the density perturbations are small, $\delta \ll 1$. Moreover, the Newtonian perturbation theory can be used on sub-horizon scales only. The fluid can then be described in co-moving coordinates using the continuity equation

$$\frac{\partial \delta}{\partial t} + \frac{1}{a}\nabla \cdot [(1+\delta)\mathbf{v}] = 0, \tag{5.10}$$

and Euler equation

$$\frac{\partial \mathbf{v}}{\partial t} + H\mathbf{v} + \frac{1}{a}(\mathbf{v}\cdot\nabla)\mathbf{v} = -\frac{1}{a}\nabla\phi - \frac{\nabla P}{a\overline{\rho}(1+\delta)}. \tag{5.11}$$

The gravitational potential ϕ can be given by the Poisson equation

$$\nabla^2\phi = 4\pi G\overline{\rho}a^2\delta. \tag{5.12}$$

Since the perturbation δ and velocity $\mathbf{v}$ are small, the nonlinear terms can be neglected, and the fluid equations can be combined to get

$$\frac{\partial^2\delta}{\partial t^2} + 2H\frac{\partial\delta}{\partial t} = \delta\left(4\pi G\overline{\rho} + \frac{c_s^2k^2}{a^2}\right), \tag{5.13}$$

where c_s is the sound speed and k is the wave number. The second term on the left-hand side of this equation is the Hubble drag term, which suppresses the growth of perturbations due to the expansion of the Universe. The first term on the right-hand side is the gravitational term, which causes the dark matter perturbation growth. The second term on the right-hand side is a pressure term, which describe the effect of baryonic matter. Eq. 5.13 has two solutions, and one of them grows with time. The limiting wavelength for structure growth is the Jeans length

$$\lambda_J = \frac{2\pi}{k_J} = c_s \sqrt{\frac{\pi}{G\rho}}. \tag{5.14}$$

The corresponding mass is the Jeans mass

$$M_J = \frac{4\pi}{3}\rho_0 \left(\frac{\lambda_J}{2}\right)^3. \tag{5.15}$$

Fluctuations with mass higher than the Jeans mass can form structures. Before the recombination baryonic matter fluctuates with radiation. At this point the sound speed is relativistic, and the Jeans mass very high, $10^{15} M_\odot$. The mass of a sub-horizon-sized density fluctuation is always less than the Jeans mass, and cannot form structures. At recombination the baryonic component behaves like a mono-atomic gas. The Jeans mass drops to $\sim 10^5 M_\odot$, and fluctuations on small scales start growing. The Jeans mass at this epoch corresponds closely to the mass of globular clusters, which are among the oldest objects in the Universe. Since dark matter does not interact with radiation, its density fluctuations have been growing before recombination. Baryons can then fall into the potential wells of dark matter.

5.3 Nonlinear evolution

While growth of small fluctuations can be described by a linear theory, at later phase the growth turns non-linear. Non-linear growth cannot be solved analytically. However, growth can be approximated by several models, such as the spherical top-hat model, the Press-Schechter formalism, and the Zel'dovich approximation. The most realistic description of the later phases of structure formation can be obtained by cosmological simulations.

5.3.1 Spherical top-hat model

For a simple model, we can assume a spherical over-dense volume. Because the gravitational force inside a sphere depends only on the matter inside, the over-dense region behaves like a small closed universe. Solution for Friedmann equations (Eqs. 5.2 and 5.3) shows that a closed universe would first expand, then turn around, start to shrink,

and finally collapse. Because the perturbations are not exactly spherical, this collapse does not happen, but instead the perturbation virializes.

The model provides a prediction of the over-density of the collapsed sphere compared to the background universe. In a matter-dominated universe at the time of the turnaround the over-density is $\delta(t_{\mathrm{max}}) \approx 4.55$. Virialization is expected to happen halfway between the turnaround and collapse, when the over-density is $\delta(t_{\mathrm{vir}}) \approx 147$. It is possible that this time is not enough for virialization, but it is eventually achieved at the collapse time (Peacock 1999). In this case the density contrast becomes ≈ 178.

The spherical model is naturally only an approximation: the density perturbations in the early universe are not always spherical as we assumed. What happens after virialization is even more complicated. The newly formed body continues to attract matter by its gravity. Spherical approximations of this phase have been studied e.g. by Gunn & Gott (1972) and Bertschinger (1985), but a more realistic modeling can be achieved by using numerical simulations. In cosmological simulations dark matter halos are often defined using the over-density of 178 (possibly rounded up to 200) that was obtained from the spherical model as the limit.

5.3.2 Press-Schechter formalism

Press & Schechter (1974) developed a model that is based on an early universe that is described by a Gaussian random field of density perturbations. The fraction of mass in massive halos is assumed to be related to the fraction of the volume in which the smoothed initial density field is above some threshold density. Most commonly the threshold is taken from the spherical top-hat model. At the critical density contrast, the region is assumed to collapse rapidly and independently of its surroundings. After the collapse, the internal structure of the clump is lost, and on the outside the region behaves like a single body of enclosed mass. This simplification makes it possible to use linear equations to describe the further evolution.

The Press-Schechter formalism gives an estimate of mass function of the collapsed objects. However, this mass function predicts too many low-mass (Peacock & Heavens 1990) and too few high mass objects.

5.3.3 Zel'dovich approximation

The Zel'dovich approximation (Zel'dovich 1970) describes the beginning of non-linear evolution, or the "mildly non-linear regime". The approximation can be used on scales much smaller than the size of horizon during the matter-dominated era.

The basic assumption is that the density contrasts are distributed on a Gaussian field. Particles in this Gaussian distribution have initial peculiar velocities, which they maintain while they follow straight paths through space. The collapse happens first along one direction, and the first non-linear structures that form are therefore two-dimensional sheets, Zel'dovich pancakes. This approximation leads to the web-like structure of the

Universe as described in Sect. 3.2. After these first structures, the approximation is no longer valid, and other methods must be used. The Zel'dovich approximation can be used as the initial setup for simulations.

5.3.4 Cosmological simulations

The only way to study the nonlinear structure formation accurately is through numerical simulation. Cosmological simulations are based on an assumption that the dominant mass component is the cold dark matter (CDM). CDM is assumed to be made of elementary particles that interact only through gravitation. The matter particles are collisionless and can be represented by a set of discrete point particles (Springel et al. 2005b).

Since the first simulations used for modeling formation and evolution of galaxies and clusters (e.g. Holmberg 1941; Peebles 1970; Press & Schechter 1974), the methods and computing power have been greatly improved. Currently the most widely used cosmological simulation is the Millennium Run. The first results were obtained by following 2160^3 particles in a cubic region of 500 h^{-1}Mpc on a side starting from redshift $z = 127$ (Springel et al. 2005b). The simulation was further expanded into the Millennium-II Simulation (MS-II), which was smaller in size (100 h^{-1}Mpc box), but had an improved mass and spatial resolution (Boylan-Kolchin et al. 2009). The most recent cosmological simulation is the Bolshoi simulation, which uses 2048^3 particles in a box of 250 h^{-1}Mpc (Klypin et al. 2011). The improvement compared to the Millennium Simulations is the use of more accurate and up to date cosmological parameters.

Dark matter halos were found during the simulations using the friends-of-friends (FoF) algorithm often defined using the virialization criteria found from spherical collapse model. Subsequently, galaxy sized gravitationally bound subhalos are extracted from the FoF halos. Figure 5.2 shows the evolution of the largest halo in the MS-II. The progenitor of the halo is shown on three co-moving scales and at four redshifts. The figure shows a web-like large-scale structure very similar to the observed large-scale structure discussed in Sect. 3.2.

While dark matter simulations are generally in agreement with the mass function found from observations, baryonic processes that determine galaxy properties are much more complicated to model. Hydrodynamical simulations provide a useful tool to study these processes, but unfortunately such calculations are too costly for computing in cosmological scales with high mass resolution. Zoom-in simulations of individual objects are required to study galaxy formation in detail (e.g. Johansson et al. 2012).

The OverWhelmingly Large Simulations (OWLS) project combines a number of hydrodynamical simulations with varying box sizes and resolutions. Each simulation is repeated many times, changing the numerical parameters for every run to determine which processes are dominant in galaxy evolution (Schaye et al. 2010).

One way to overcome the problem of limited computing power is to use the halo occupation model (HOD) to populate the dark matter halos with galaxies. In this model halo assembly depends only on the mass of the halo, not its environment. Another widely

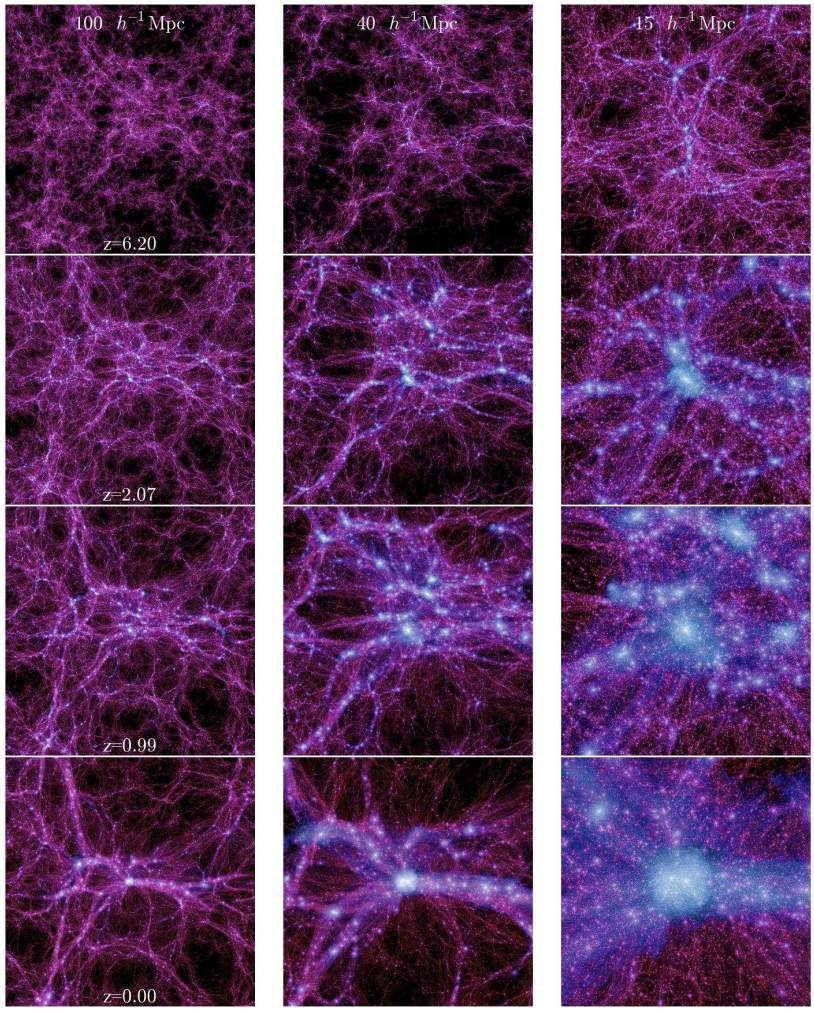

Figure 5.2: *Time evolution of a dark matter halo in the MS-II. The halo is shown on three comoving scales: 100, 40, and 15 h^{-1}Mpc, with slice thickness 15, 10, and 6 h^{-1}Mpc respectively. Figure from Boylan-Kolchin et al. (2009).*

used method to study galaxy evolution on cosmological scale are semi-analytic models (SAM).

CHAPTER 6
Galaxy evolution

The Fifth, who chanced to touch the ear,
Said: "E'en the blindest man
Can tell what this resembles most;
Deny the fact who can,
This marvel of an Elephant
Is very like a fan!"

The Blind Men and the Elephant by John Godfrey Saxe

6.1 Semi-analytic models

Galaxy evolution is usually studied using cosmological dark matter simulations, together with semi-analytic models. White & Rees (1978) first suggested that galaxy formation would be driven by the formation of dark matter halos through gravitational collapse. Galaxies form in dark matter halos following the radiative cooling of baryons. White & Frenk (1991) added models for physical processes affecting the evolution, such as star-formation, stellar populations, and cooling of gas.

Semi-analytic models are applied in a simulation, where the formation history of each dark matter halo is known in the form of a merger tree. At early stages of galaxy formation, baryonic matter is assumed to be in the form of gas that has the same spatial distribution as the dark matter. As the dark matter gathers in halos, the gas falls into the gravitational potential of the dark halo. While falling, the gas is heated by shocks. This process forms a hot gas halo.

Gas in the hot gas halo cools primarily by two mechanisms: emission of photons following transitions between energy levels and bremsstrahlung radiation as electrons are accelerated in an ionized plasma (Baugh 2006). Cooling time can be estimated as

$$t_{\text{cool}}(r) = \left(\frac{3}{2}\frac{\rho_{\text{gas}} k T_{\text{vir}}}{\mu m_{\text{H}}}\right) / \left(\rho^2_{\text{gas}} \Lambda(T_{\text{vir}}, Z_{\text{gas}})\right), \tag{6.1}$$

where ρ_{gas} is the gas density and Λ is the cooling function, which is a function of the temperature and metallicity Z_{gas}. The cooling model can further be modified by taking into account effects like the suppression of cooling by a background of photo-ionizing radiation in low mass halos. In massive halos cooling can be suppressed by heating of the gas through supernova explosions, by thermal conduction of energy from the outer to the inner parts of the halo, and by energy released from the accretion of material onto

a central black hole. When the gas cools, it settles in the center of the halo and forms a rotating disk. As a result of conservation of angular momentum in the disk, the rotation curves become flat (Fall & Efstathiou 1980). This slow process of a collapse of a gas cloud leads to the formation of disk galaxies.

Cold gas is needed for star formation. Based on observations of star formation in the nearby universe, we know that stars form in clouds of very cold molecular gas. However, a detailed theory of star formation has not yet been found. Because of this, the approach used in semi-analytical models is a simple estimate:

$$\dot{M}_* = \frac{M_{\text{cold}}}{\tau_*}, \tag{6.2}$$

where $\dot{M}_*$ is the star-formation rate that depends on the amount of cold gas M_{cold} and the star-formation timescale τ_* (Okamoto 2008).

Mergers of dark matter halos are the driving force of structure formation. These mergers also affect the galaxies and the baryonic matter in the halos. The hot gas halos follow the dark matter and form a new hot gas halo immediately after a merger. On the other hand, galaxies take a longer time to merge: The less massive galaxy becomes a satellite of the more massive one. It will orbit the central galaxy with an orbit that decays due to dynamical friction. A simplified equation for the force from dynamical friction has the form

$$f_d \simeq C\frac{G^2M^2\rho}{v_M^2}, \tag{6.3}$$

where M is the mass of the satellite galaxy and v_M is its velocity. Density of the surrounding material is ρ and C is a function that depends on the velocity of the satellite compared to the velocity dispersion of the surrounding medium. As the friction force depends on v^{-2}, objects that move slowly experience more dynamical friction than objects that move fast. Since galaxies in groups move more slowly than galaxies in clusters, dynamical friction is more efficient in groups. Finally, when the dynamical friction has reduced the orbit enough, the satellite may merge to the central galaxy (Binney & Tremaine 1987).

Mergers of galaxies can be divided into minor mergers, where the satellite galaxy is considerably less massive than the central galaxy, and major merger, where two galaxies of approximately equal mass merge. The division between major and minor mergers is usually drawn at a mass ratio of 3:1. Major mergers alter the dynamics in galaxies dramatically, and often cause gas inflows and trigger starburst activity (Mihos & Hernquist 1996). The role of mergers in galaxy evolution will be discussed in more detail in Sect. 6.2.1.

In their basic model of galaxy evolution White & Rees (1978) found that the luminosity function for modeled galaxies gets steeper in the low-mass end than the observed luminosity function. This can be corrected by adapting feedback processes that affect the evolution of galaxies. Feedback processes include various physical phenomena that

affect heating and cooling the gas in a galaxy. The most important feedback process is the effect of supernovae, which heat the gas and drive it out of the galaxy in a galactic wind (Larson 1974; Dekel & Silk 1986). Besides the supernova feedback, low-mass galaxies may also be affected by UV heating by photoionization. This heats the gas enough to expel it into the intergalactic medium (Finlator et al. 2011).

The UV and supernova feedback may correct the low-mass end of the luminosity function, but they do not affect the excess of massive galaxies (Benson et al. 2003). Another type of feedback is needed to correct the high-mass end. This can be done with an AGN feedback (Croton et al. 2006). AGN feedback in massive galaxies will be discussed in Sect. 6.2.2.

6.2 The role of AGNs

6.2.1 Mergers and quasar activity

The tight correlation between the mass of a galaxy and the mass of the supermassive black hole in its center has lead to a conclusion that the galaxy and the black hole co-evolve. The importance of mergers in galaxy evolution, on the other hand, raises a question of what happens to the black holes when their host galaxies merge. Kauffmann & Haehnelt (2000) suggested that quasars can be triggered by major mergers. Springel et al. (2005a) modeled star formation and black hole accretion in hydrodynamical simulations of merging galaxies. They found that in major mergers of gas-rich galaxies the black hole can expel gas from the center in a powerful outflow. The tidal interaction in the merger triggers intense nuclear inflows of gas, which leads to starbursts and AGNs. When the accreting black hole has grown to a critical size, feedback terminates its growth and expels gas from the central region of the galaxy. Through this method, the black hole can be responsible for quenching star formation and moving the galaxy into the red sequence. Johansson et al. (2009) compared mergers with different mass ratios and found that the star formation can be terminated in a major merger, but not in minor mergers, where the mass ratio is 3:1 or higher.

Figure 6.1 shows a merger simulation by Hopkins et al. (2006). Each panel shows a snapshot of the simulation at a certain time, and colors refer to the gas fraction. As outlined by Hopkins et al. (2008), the process starts from disk galaxies in small groups. Galactic disks grow quiescently through secular evolution. Pseudobulges and bars may form, and low-luminosity AGN activity is also possible e.g. through disk instabilities. When a merger between two gas-rich disk galaxies begins, the galaxies first affect the dynamics of each others by tidal torques (time $T = 0.39$ Gyr in Fig. 6.1). These may excite some enhanced star formation and black hole accretion, but the effect is weak, and they usually do not trigger AGNs.

When the galaxies reach the point of the final merger, massive inflows of gas trigger starbursts. The merging galaxies can be observed as ultra-luminous infrared galaxies (ULIRG). This phase corresponds to approximately times $T = 1.11$ to $T = 1.30$ Gyr

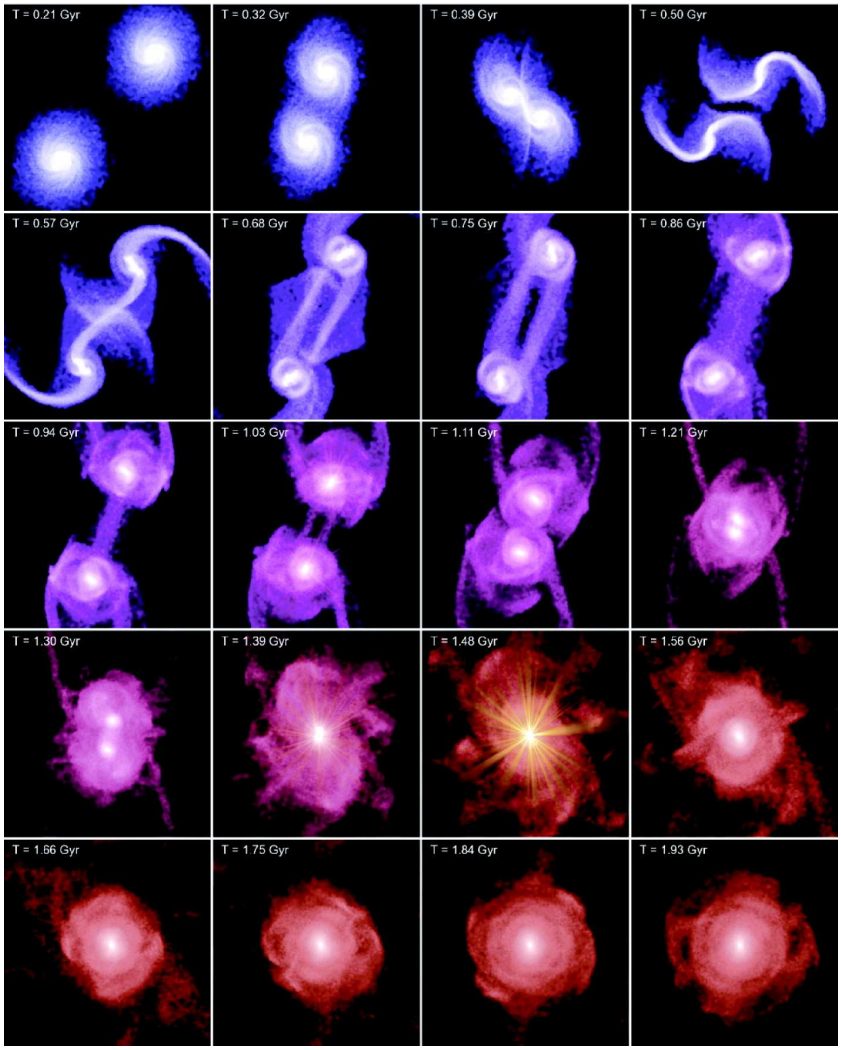

Figure 6.1: *Time sequence of a merger simulation. Colors indicate the gas fraction from 20 % (blue) to 5 % (red), and brightness gives the projected stellar mass density. Nuclear point sources (possible AGNs) are shown at T =1.03, 1.39, and 1.48. Figure from Hopkins et al. (2006).*

in Fig. 6.1. The black hole grows, but a large amount of gas and dust obscure the AGN from view. The starburst consumes gas, and the feedback from the black hole starts to expel the rest of it. In this short blowout phase the obscuring material is removed, and an optical quasar becomes visible ($T = 1.48$ Gyr in Fig. 6.1). At this point the merger is complete and the spheroid has formed. During the quasar phase, the black hole keeps growing by accreting gas. When the gas is consumed and dispersed, the activity declines. The remaining galaxy is an elliptical with little gas and star formation.

This picture of quasars triggered by mergers is simplified and still requires more

studies for confirmation. As Hopkins et al. (2008) points out, especially the low-luminosity quasars and Seyfert galaxies are more likely to be triggered through secular processes. This means that gas starts to accrete onto the black hole through instabilities in the disk or the bar of the galaxy. Some of the observational evidence also disagrees with the merger scheme: Szomoru et al. (2012) found that the density profiles of massive early type galaxies are not as disturbed as they were if major gas-rich mergers had contributed significantly to their evolution after $z \sim 2$. Furthermore, Cisternas et al. (2011) found no sign of mergers in AGN host galaxies at redshifts of $z \sim 0.3$–1.0. Based on this result, they conclude that at least for the last 7.5 Gyr, major merging has not been the most relevant mechanism in the triggering of AGNs.

6.2.2 Radio mode feedback in elliptical galaxies

Without an appropriate feedback process, semi-analytical models tend to produce an excess of massive galaxies (Benson et al. 2003). Croton et al. (2006) suggested that a suitable feedback mechanism can be provided by radio sources. While the 'quasar mode' AGNs are triggered through mergers of galaxies and work by expelling gas from the central regions of the galaxy so that it is no longer available for cooling, the 'radio mode' is activated as a result of a continual and quiescent hot gas accretion onto the black hole. The feedback energy from the radio-mode black hole then heats the surrounding gas and prevents it from cooling.

In the radio mode feedback, energy is transferred by jets. Jets are radio luminous because of the synchrotron radiation from electrons that are accelerated in shocks. Compared to accretion disks, jets produce relatively low luminosities. In the radio mode feedback, the accretion rates are lower than in the quasar mode. An accretion disk may not be formed at all, and the accreting material can be carried out by the jets. Because of this, jets can be considered a radiatively inefficient or mechanical feedback method. Despite the inefficiency, radio jets are important for energy input of their host galaxies because the energy is deposited locally in the galaxy, instead of being driven away. The way the energy released in a radio mode AGN affects the galaxy is that the radiation heats the surrounding gas (Cattaneo & Best 2009). Therefore, the radio mode feedback suppresses cooling in massive halos, and thus regulate their growth.

To summarize the role of AGNs in galaxy evolution, quasars are triggered by major mergers of gas-rich galaxies, and they are responsible for expelling the gas, and thus terminating star formation. They are responsible for turning galaxies from the blue cloud to the red sequence. Radio galaxies, on the other hand, get active through a steady inflow of gas onto the black hole. Their jets provide mechanical feedback that warms the surrounding gas. Through this feedback process radio jets regulate the masses of old red galaxies.

6.3 Galaxies and their environment

Red and blue galaxies have different environments. Red galaxies are located in denser regions than the blue ones (Gómez et al. 2003). The same can be seen with AGN: radio galaxies tend to be more clustered than quasars (see more details in Chapters 3 and 4). This dependency between the galaxy type and the environment suggests that the environment may also affect the evolution of galaxies.

There are several ways through which the environment can affect the evolution of a galaxy. Galaxy mergers depend on the environment. Mergers are most efficient in small groups of galaxies because in rich clusters the velocities of galaxies are too high for merging (Hopkins et al. 2008). This is due to the dynamical friction, which is proportional to v^{-2}, and therefore more efficient when the velocities are low. Ram pressure stripping may remove gas from a galaxy that moves in a cluster through intra-cluster medium (Gunn & Gott 1972). Morphology of galaxies may be transformed through galaxy harassment in high speed galaxy encounters (Moore et al. 1996).

A usual assumption in semi-analytic models is to ignore correlations between different spatial scales. This means that there should be no correlation between halo formation and its large-scale environment (Sheth & Tormen 2004). However, Sheth & Tormen (2004) found that the environment does have an effect on the halo population. Close pairs of halos form at higher redshifts than more widely separated halo pairs, indicating that halos in dense regions form at earlier times than halos of the same mass in less dense regions. The significance of the environment was supported by the results of Gao et al. (2005), who found that the oldest 10 % of halos are more than five times more strongly correlated than the youngest 10 % with the same mass, indicating an assembly bias in halo formation. This means that galaxies in dense environments evolve to a certain stage earlier than galaxies in low-density environments.

If old halos are more clustered than the young, it is expected for the galaxies in dense environments to be older. Since red elliptical galaxies and radio galaxies are at a later phase of galaxy evolution than star-forming galaxies and quasars, they can be considered older. This could explain the denser environments of red galaxies at low redshifts. Galaxies in dense environments may have evolved to the quasar phase earlier, and have ended their star formation at that time. This is supported by observations: Porciani et al. (2004) calculated a projected correlation function of quasars to study their clustering. They found that quasars at redshift $z_{\text{eff}} = 1.89$ are considerably more clustered than quasars at redshift $z_{\text{eff}} = 1.47$.

Using semi-analytic models, Cen (2011) found that while the large halos form, gas in them is heated. As a result, the entropy of gas in high-density regions gets too high to cool to feed galaxies. This leads to cold gas starvation in dense regions earlier than in low-density regions. At the present epoch, star-formation is suppressed in high-density environments but still efficient in low-density regions.

Hickox et al. (2009) summarize the environment-dependent evolution scenario as shown in Fig. 6.2. If the initial halo mass was high, the galaxy at low redshift is observed

in a dense environment. Because in high-mass halos galaxies evolve to a certain phase earlier, these galaxies become quasars at higher redshifts than galaxies initially in low-mass halos. A typical halo mass at the quasar phase is 10^{12} to $10^{13} M_{\odot}$. Galaxies in halos with initially low mass are observed as quasars at low redshifts or still as star-forming galaxies. Galaxies in halos with high initial masses have become red, passive galaxies or radio galaxies by the present time. This is consistent with our results in Papers II and III. At low redshifts quasars are in low-density environments. Radio galaxies, on the other hand, are found in denser regions. We concluded that the since the number of quasars has declined from the peak at $z \approx 2$, the ones at low redshifts are among the "slowest" to evolve.

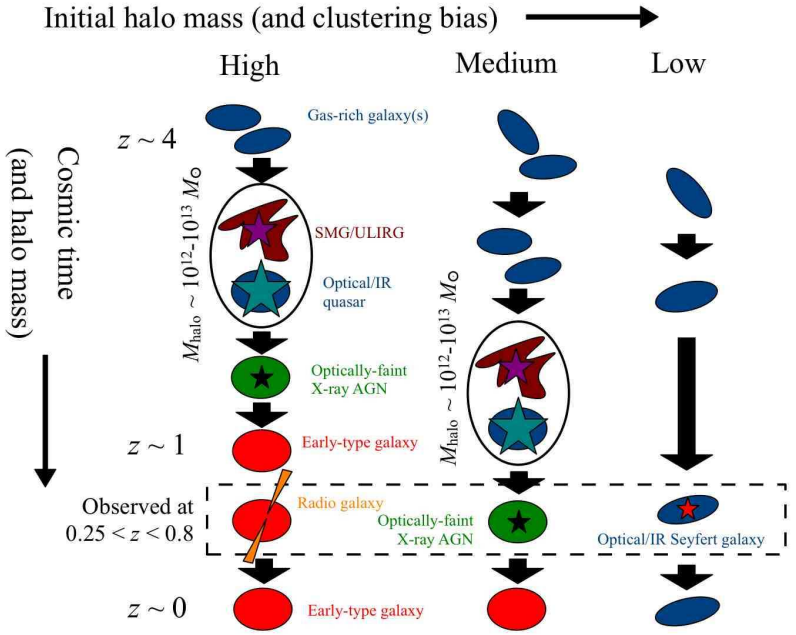

Figure 6.2: *Schematic for a simple picture of AGN and host galaxy evolution. Evolution is shown for three classes of initial halo mass. Colors in the figure represent the colors of the host galaxy. Figure from Hickox et al. (2009).*

CHAPTER 7
Summary of the papers

The Sixth no sooner had begun
About the beast to grope,
Then, seizing on the swinging tail
That fell within his scope,
"I see," quoth he, "the Elephant
Is very like a rope!"

The Blind Men and the Elephant by John Godfrey Saxe

In the papers in this thesis we studied the environments of active galaxies at low redshifts on different scales. A general aim has been to characterize the environmental density on the group and the supercluster scales. Paper I is a detailed study of one BL Lac object on cluster scale. In Paper II we studied the environments of quasars compared to luminous non-active galaxies. Paper III compares the large-scale environments of different types of AGN. In paper IV, the point of view is extended from AGN to star-forming and passive galaxies. We study the group and the supercluster scales together to see which of these scales is more important for determining the properties of galaxies.

7.1 Paper I

In this paper we studied the environment of BL Lac object RGB 1745+398. The target was selected for a closer study because its host galaxy is the central galaxy of a cluster working as a strong gravitational lens. This made it possible to study the cluster in detail and get an accurate estimate for its mass.

We used optical spectra of nine galaxies belonging to the cluster to measure the velocity dispersion of the cluster. The redshift of the cluster is 0.268, and its velocity dispersion $\left(470^{+190}_{-110}\right)\,\mathrm{km\,s^{-1}}$. Using gravitational lensing we found that the mass of the cluster is $M_{500} = \left(4^{+3}_{-2}\right) \times 10^{14} M_{\odot}$, indicating a massive cluster. To measure the richness of the cluster, we calculated the galaxy-BL Lac spatial covariance function amplitude, $B_{\mathrm{gb}} = (600 \pm 200)\,\mathrm{Mpc}^{1.77}$. Richness is consistent with the mass and velocity dispersion of the cluster.

This is the most detailed study made of the cluster-scale environment of a BL Lac object. The rarity of strong gravitational lenses limits the mass determination for other clusters with AGNs. However, the other methods used in this paper, spectroscopy of cluster member galaxies and richness estimates, can be used for other clusters with AGNs as well. A possible future project could be to study the dynamics of groups or clusters with AGNs in more detail.

7.2 Paper II

With the SDSS, it has now become possible to study the most nearby quasars together with a large number of galaxies. The complete volume and magnitude-limited galaxy catalogs based on the SDSS reach redshift $z \sim 0.2$ corresponding to a distance of 500 Mpc. Inside this upper limit, the SDSS fifth data release quasar catalog contained 174 quasars. We studied the environments of these quasars on large scales.

We found that compared to luminous non-active galaxies, quasars had less neighboring galaxies on scales of a few Mpc. Quasars were typically located 10 to 15 Mpc from rich groups of galaxies, groups closer to quasars being poorer and less massive. Clusters in the environments of quasars were later studied by Harris (2012), who found that at redshifts $0.2 < z < 0.4$ quasars lie closer to rich clusters than quasars in our sample. This issue may need further studies to confirm whether the difference between our result and theirs is an evolutionary effect or caused by selection effects.

Finally, we used a luminosity-density field to study the environments on supercluster scale. We found that quasars are typically located at the edges of superclusters or in filaments. The average environmental density of a quasar was 2.4 times the mean density, which is considerably lower than supercluster densities (> 4.6 times the mean density). No quasars were found in supercluster core regions with densities more than ten times the mean density. We concluded that the low-redshift quasars may be in the low-density environments because galaxies in these environments evolve later. These galaxies have therefore only recently evolved to the phase where triggering of quasars is likely.

7.3 Paper III

We continued the work done in Paper II by extending the volume of our analysis using luminous red galaxies (LRGs) as our control sample instead of all galaxies. LRGs are the most luminous galaxies, and therefore, they can be observed to a larger distance than normal galaxies. We constructed a luminosity-density field based on the LRGs to study the large-scale environments of AGN at redshift $z < 0.4$.

The larger volume increased our quasar sample to more than 3000 quasars. We could now also study other types of AGN: Seyfert galaxies, radio galaxies, and BL Lac objects. We found that quasars and Seyfert galaxies are mostly located in low-density environments, while radio galaxies are more likely to be found in superclusters. BL Lac objects are found both in void regions and in superclusters.

Our results show that the environments of AGN are different on the supercluster scale. Earlier results on smaller scale (e.g. Hickox et al. 2009) have shown similar differences between quasars and radio galaxies: radio galaxies are in richer groups or clusters. The agreement of the group-scale and the supercluster-scale is expected, since superclusters are made of groups, and groups in dense large-scale environments are richer than groups in emptier regions. The result supports the model of galaxy evolution, where

quasars make an earlier phase of galaxy evolution than radio galaxies. If the dense areas evolve faster to the epoch of radio galaxies, we are more likely to find low-redshift radio galaxies in denser environments than quasars or Seyfert galaxies.

7.4 Paper IV

The results of Paper III raised a question of the significance of different scales of environments. The differences between radio and quasar-type AGN, as well as passive and star-forming galaxies, can be seen both on group scale and on supercluster scale. In this paper we studied these two scales together to see which of these scales is more important for galaxy evolution.

We divided the galaxies in the SDSS galaxy catalog in different categories based on their morphology and spectral properties. Our sample included spiral and elliptical galaxies based on morphology, and passive, star-forming and AGN galaxies divided by their spectral properties. We studied the fractions of these different types of galaxies in groups with different richnesses and in different large-scale environments.

We found that galaxies in equally rich groups are more likely to be passive ellipticals if they are in supercluster environments than if they are in lower-density environments. When the large-scale density is the same, the fractions of star-forming and passive galaxies depend on the group richness in groups with less than approximately ten galaxies. The group richness at which the passive galaxies become more numerous than star-forming galaxies depends on the large-scale environment. This means that the large-scale environment affects galaxies independently of the group richness.

This study suggests that the large-scale environment is important for galaxy evolution. The result supports the theory that dense regions evolve earlier than the low-density areas. We can conclude that the observed differences between the environments of different types of galaxies and different types of AGN are a result of the halo assembly that affects the large-scale density, and not only a result of local group-scale variation.

CHAPTER 8
Conclusions

Recent theoretical and observational studies have now started to provide a more complete picture of galaxies and their evolution. The results of this dissertation advance our knowledge on this issue by connecting two important factors affecting galaxy evolution: nuclear activity and the large-scale environment.

Different types of AGN are believed to be typically triggered at different phases of galaxy evolution. Quasar activity is usually found in young galaxies, while radio galaxies are typically old. Because of this, AGN could be seen as indicators of galaxy populations of a certain evolutionary phase. On the other hand, galaxies in different environments evolve differently. In dense environments galaxies are more often red ellipticals with little star formation.

In Papers II and III we found that at low redshifts, quasars are usually found in low-density large-scale environments. Radio galaxies are more concentrated in high-density environments. The results in Paper IV suggest that the number of galaxies that are star-forming is affected by the large-scale environment, and not only by the local, group scale environment.

The large-scale density reflects the initial mass of the dark matter halos in which the galaxies evolve. The difference in galaxy and AGN populations in high and low-density large-scale environments can be interpreted as a dependency of galaxy evolution on the initial halo mass. If a galaxy reaches a certain phase of evolution earlier in a more massive halo, the galaxies we observe at low redshifts in dense environments are more likely to have evolved to a more mature phase than galaxies in low-density environments.

A possible future project would be to study the small and large-scale environments of simulated galaxies in cosmological simulations. With the simulations we could study the evolutionary paths leading to different galaxies and see how they depend on the halo mass. Another possibility would be to study the effects of small-scale environments on galaxies using deep spectroscopical observations. This way we could get more accurate information on groups and clusters of galaxies than by using the SDSS data, which is limited to the most luminous galaxies. The studies presented in this dissertation have given support for the importance of the large-scale environment for the evolution of activity in galaxies. The results set a background for more detailed studies in the future.

Bibliography

Abell, G. O. 1958, ApJS, 3, 211

Aihara, H., Allende Prieto, C., An, D., et al. 2011, ApJS, 193, 29

Angel, J. R. P. & Stockman, H. S. 1980, ARA&A, 18, 321

Antonucci, R. 1993, ARA&A, 31, 473

Bahcall, J. N., Schmidt, M., & Gunn, J. E. 1969, ApJ, 157, L77

Bahcall, N. A. 1977, ApJ, 217, L77

Bahcall, N. A. 1981, ApJ, 247, 787

Bahcall, N. A., Lubin, L. M., & Dorman, V. 1995, ApJ, 447, L81

Baldwin, J. A., Phillips, M. M., & Terlevich, R. 1981, PASP, 93, 5

Bamford, S. P., Nichol, R. C., Baldry, I. K., et al. 2009, MNRAS, 393, 1324

Barkana, R. & Loeb, A. 2001, Phys. Rep., 349, 125

Baugh, C. M. 2006, Reports on Progress in Physics, 69, 3101

Bender, R. 1988, A&A, 193, L7

Benson, A. J., Bower, R. G., Frenk, C. S., et al. 2003, ApJ, 599, 38

Bertschinger, E. 1985, ApJS, 58, 39

Best, P. N. & Heckman, T. M. 2012, MNRAS, 421, 1569

Binney, J. & Tremaine, S. 1987, Galactic dynamics (Princeton)

Blanton, M. R., Eisenstein, D., Hogg, D. W., Schlegel, D. J., & Brinkmann, J. 2005, ApJ, 629, 143

Blanton, M. R., Hogg, D. W., Bahcall, N. A., et al. 2003, ApJ, 594, 186

Bolton, J. G., Stanley, G. J., & Slee, O. B. 1949, Nature, 164, 101

Boylan-Kolchin, M., Springel, V., White, S. D. M., Jenkins, A., & Lemson, G. 2009, MNRAS, 398, 1150

Brinchmann, J., Charlot, S., White, S. D. M., et al. 2004, MNRAS, 351, 1151

Butcher, H. & Oemler, Jr., A. 1978, ApJ, 219, 18

Cattaneo, A. & Best, P. N. 2009, MNRAS, 395, 518

Cen, R. 2011, ApJ, 741, 99

Cisternas, M., Jahnke, K., Inskip, K. J., et al. 2011, ApJ, 726, 57

Coldwell, G. V. & Lambas, D. G. 2006, MNRAS, 371, 786

Colless, M., Dalton, G., Maddox, S., et al. 2001, MNRAS, 328, 1039

Couch, W. J., Ellis, R. S., Sharples, R. M., & Smail, I. 1994, ApJ, 430, 121

Cowie, L. L., Songaila, A., Hu, E. M., & Cohen, J. G. 1996, AJ, 112, 839

Croton, D. J., Springel, V., White, S. D. M., et al. 2006, MNRAS, 365, 11

Davies, R. L., Efstathiou, G., Fall, S. M., Illingworth, G., & Schechter, P. L. 1983, ApJ, 266, 41

Davis, M. & Huchra, J. 1982, ApJ, 254, 437

De Robertis, M. M., Yee, H. K. C., & Hayhoe, K. 1998, ApJ, 496, 93

de Vaucouleurs, G. 1948, Annales d'Astrophysique, 11, 247

Dekel, A. & Silk, J. 1986, ApJ, 303, 39

Donoso, E., Li, C., Kauffmann, G., Best, P. N., & Heckman, T. M. 2010, MNRAS, 407, 1078

Dressler, A. 1980, ApJ, 236, 351

Dressler, A., Smail, I., Poggianti, B. M., et al. 1999, ApJS, 122, 51

Driver, S. P., Allen, P. D., Graham, A. W., et al. 2006, MNRAS, 368, 414

Dultzin-Hacyan, D., Krongold, Y., Fuentes-Guridi, I., & Marziani, P. 1999, ApJ, 513, L111

Edge, D. O., Shakeshaft, J. R., McAdam, W. B., Baldwin, J. E., & Archer, S. 1959, MmRAS, 68, 37

Einasto, J., Einasto, M., Saar, E., et al. 2007a, A&A, 462, 397

Einasto, J., Einasto, M., Tago, E., et al. 2007b, A&A, 462, 811

Einasto, J., Hütsi, G., Einasto, M., et al. 2003, A&A, 405, 425

Einasto, M. & Einasto, J. 1987, MNRAS, 226, 543

Einasto, M., Einasto, J., Tago, E., et al. 2007c, A&A, 464, 815

Einasto, M., Liivamägi, L. J., Tempel, E., et al. 2011, ApJ, 736, 51

Einasto, M., Saar, E., Liivamägi, L. J., et al. 2007d, A&A, 476, 697

Einasto, M., Saar, E., Martínez, V. J., et al. 2008, ApJ, 685, 83

Einstein, A. 1917, Sitzungsberichte der Königlich Preußischen Akademie der Wissenschaften (Berlin), Seite 142-152., 142

Ellingson, E., Yee, H. K. C., & Green, R. F. 1991, ApJ, 371, 49

Faber, S. M. & Jackson, R. E. 1976, ApJ, 204, 668

Fall, S. M. & Efstathiou, G. 1980, MNRAS, 193, 189

Fanaroff, B. L. & Riley, J. M. 1974, MNRAS, 167, 31P

Ferrarese, L. & Merritt, D. 2000, ApJ, 539, L9

Finlator, K., Davé, R., & Özel, F. 2011, ApJ, 743, 169

Fisher, K. B., Bahcall, J. N., Kirhakos, S., & Schneider, D. P. 1996, ApJ, 468, 469

Fukugita, M., Nakamura, O., Turner, E. L., Helmboldt, J., & Nichol, R. C. 2004, ApJ, 601, L127

Gao, L., Springel, V., & White, S. D. M. 2005, MNRAS, 363, L66

Gavazzi, G., Fumagalli, M., Cucciati, O., & Boselli, A. 2010, A&A, 517, A73

Gladders, M. D. & Yee, H. K. C. 2000, AJ, 120, 2148

Gómez, P. L., Nichol, R. C., Miller, C. J., et al. 2003, ApJ, 584, 210

Gott, III, J. R., Jurić, M., Schlegel, D., et al. 2005, ApJ, 624, 463

Govoni, F., Falomo, R., Fasano, G., & Scarpa, R. 2000, A&AS, 143, 369

Greenstein, J. L. 1963, Nature, 197, 1041

Gunn, J. E. & Gott, III, J. R. 1972, ApJ, 176, 1

Gursky, H., Kellogg, E., Murray, S., et al. 1971, ApJ, 167, L81

Hamilton, A. J. S. 1988, ApJ, 331, L59

Hardcastle, M. J., Evans, D. A., & Croston, J. H. 2006, MNRAS, 370, 1893

Harris, K. A. 2012, ArXiv e-prints

Hes, R., Barthel, P. D., & Fosbury, R. A. E. 1993, Nature, 362, 326

Hickox, R. C., Jones, C., Forman, W. R., et al. 2007, ApJ, 671, 1365

Hickox, R. C., Jones, C., Forman, W. R., et al. 2009, ApJ, 696, 891

Hill, G. J. & Lilly, S. J. 1991, ApJ, 367, 1

Hine, R. G. & Longair, M. S. 1979, MNRAS, 188, 111

Hinshaw, G., Weiland, J. L., Hill, R. S., et al. 2009, ApJS, 180, 225

Holmberg, E. 1941, ApJ, 94, 385

Hopkins, P. F., Hernquist, L., Cox, T. J., et al. 2006, ApJS, 163, 1

Hopkins, P. F., Hernquist, L., Cox, T. J., & Kereš, D. 2008, ApJS, 175, 356

Hoyle, F. & Vogeley, M. S. 2004, ApJ, 607, 751

Hubble, E. 1927, Contributions from the Mount Wilson Observatory, vol. 3, pp.23-28, 3, 23

Hubble, E. P. 1926, ApJ, 64, 321

Hubble, E. P. 1936, Realm of the Nebulae (Yale University Press)

Huertas-Company, M., Aguerri, J. A. L., Bernardi, M., Mei, S., & Sánchez Almeida, J. 2011, A&A, 525, A157

Hyvönen, T., Kotilainen, J. K., Falomo, R., Örndahl, E., & Pursimo, T. 2007a, A&A, 476, 723

Hyvönen, T., Kotilainen, J. K., Örndahl, E., Falomo, R., & Uslenghi, M. 2007b, A&A, 462, 525

Jõeveer, M. & Einasto, J. 1978, in IAU Symposium, Vol. 79, Large Scale Structures in the Universe, ed. M. S. Longair & J. Einasto, 241–250

Jackson, N. & Browne, I. W. A. 1990, Nature, 343, 43

Jahnke, K., Kuhlbrodt, B., & Wisotzki, L. 2004, MNRAS, 352, 399

Jarosik, N., Bennett, C. L., Dunkley, J., et al. 2011, ApJS, 192, 14

Johansson, P. H., Naab, T., & Burkert, A. 2009, ApJ, 690, 802

Johansson, P. H., Naab, T., & Ostriker, J. P. 2012, ApJ, 754, 115

Kauffmann, G. & Haehnelt, M. 2000, MNRAS, 311, 576

Kauffmann, G., White, S. D. M., Heckman, T. M., et al. 2004, MNRAS, 353, 713

Kellermann, K. I., Sramek, R., Schmidt, M., Shaffer, D. B., & Green, R. 1989, AJ, 98, 1195

Khachikian, E. Y. & Weedman, D. W. 1974, ApJ, 192, 581

Kharb, P., Lister, M. L., & Cooper, N. J. 2010, ApJ, 710, 764

Klypin, A. A., Trujillo-Gomez, S., & Primack, J. 2011, ApJ, 740, 102

Kollgaard, R. I. 1994, Vistas in Astronomy, 38, 29

Kormendy, J., Fisher, D. B., Cornell, M. E., & Bender, R. 2009, ApJS, 182, 216

Larson, R. B. 1974, MNRAS, 169, 229

Ledlow, M. J. & Owen, F. N. 1996, AJ, 112, 9

Li, C., Kauffmann, G., Wang, L., et al. 2006, MNRAS, 373, 457

Liivamägi, L. J., Tempel, E., & Saar, E. 2012, A&A, 539, A80

Lintott, C. J., Schawinski, K., Slosar, A., et al. 2008, MNRAS, 389, 1179

Longair, M. S. & Seldner, M. 1979, MNRAS, 189, 433

Madau, P., Pozzetti, L., & Dickinson, M. 1998, ApJ, 498, 106

Maloney, A. & Petrosian, V. 1999, ApJ, 518, 32

Mather, J. C., Fixsen, D. J., Shafer, R. A., Mosier, C., & Wilkinson, D. T. 1999, ApJ, 512, 511

McLure, R. J. & Dunlop, J. S. 2001, MNRAS, 321, 515

Mihos, J. C. & Hernquist, L. 1996, ApJ, 464, 641

Mo, H., van den Bosch, F. C., & White, S. 2010, Galaxy Formation and Evolution (Cambridge University Press)

Moore, B., Katz, N., Lake, G., Dressler, A., & Oemler, A. 1996, Nature, 379, 613

Mortlock, D. J., Warren, S. J., Venemans, B. P., et al. 2011, Nature, 474, 616

Niemi, S.-M., Nurmi, P., Heinämäki, P., & Valtonen, M. 2007, MNRAS, 382, 1864

Nilsson, K., Pursimo, T., Heidt, J., et al. 2003, A&A, 400, 95

Okamoto, T. 2008, in Astronomical Society of the Pacific Conference Series, Vol. 393, New Horizons in Astronomy, ed. A. Frebel, J. R. Maund, J. Shen, & M. H. Siegel, 111

Osterbrock, D. E. 1981, ApJ, 249, 462

Parker, L. C., Hudson, M. J., Carlberg, R. G., & Hoekstra, H. 2005, ApJ, 634, 806

Peacock, J. A. 1999, Cosmological Physics (Cambridge University Press)

Peacock, J. A. & Heavens, A. F. 1990, MNRAS, 243, 133

Peebles, P. J. E. 1970, AJ, 75, 13

Percival, W. J., Baugh, C. M., Bland-Hawthorn, J., et al. 2001, MNRAS, 327, 1297

Perlman, E. S. & Stocke, J. T. 1994, AJ, 108, 56

Perlmutter, S., Aldering, G., Goldhaber, G., et al. 1999, ApJ, 517, 565

Persic, M., Salucci, P., & Stel, F. 1996, MNRAS, 281, 27

Plionis, M. & Basilakos, S. 2002, MNRAS, 330, 399

Ponman, T. J., Bourner, P. D. J., Ebeling, H., & Böhringer, H. 1996, MNRAS, 283, 690

Popesso, P., Biviano, A., Böhringer, H., Romaniello, M., & Voges, W. 2005, A&A, 433, 431

Porciani, C., Magliocchetti, M., & Norberg, P. 2004, MNRAS, 355, 1010

Porter, S. C., Raychaudhury, S., Pimbblet, K. A., & Drinkwater, M. J. 2008, MNRAS, 388, 1152

Postman, M. & Geller, M. J. 1984, ApJ, 281, 95

Press, W. H. & Schechter, P. 1974, ApJ, 187, 425

Reber, G. 1944, ApJ, 100, 279

Riess, A. G., Filippenko, A. V., Challis, P., et al. 1998, AJ, 116, 1009

Sadler, E. M., Cannon, R. D., Mauch, T., et al. 2007, MNRAS, 381, 211

Schaye, J., Dalla Vecchia, C., Booth, C. M., et al. 2010, MNRAS, 402, 1536

Schechter, P. 1976, ApJ, 203, 297

Schmidt, M. 1959, ApJ, 129, 243

Schmidt, M. 1963, Nature, 197, 1040

Schmitt, J. L. 1968, Nature, 218, 663

Schneider, D. P., Richards, G. T., Hall, P. B., et al. 2010, AJ, 139, 2360

Sersic, J. L. 1968, Atlas de galaxias australes (Observatorio Astronómico)

Seyfert, C. K. 1943, ApJ, 97, 28

Sheth, R. K. & Tormen, G. 2004, MNRAS, 350, 1385

Skibba, R. A., Bamford, S. P., Nichol, R. C., et al. 2009, MNRAS, 399, 966

Skrutskie, M. F., Cutri, R. M., Stiening, R., et al. 2006, AJ, 131, 1163

Smoot, G. F., Bennett, C. L., Kogut, A., et al. 1992, ApJ, 396, L1

Snellen, I. A. G. & Best, P. N. 2001, MNRAS, 328, 897

Springel, V., Di Matteo, T., & Hernquist, L. 2005a, MNRAS, 361, 776

Springel, V., White, S. D. M., Jenkins, A., et al. 2005b, Nature, 435, 629

Stocke, J. T., Morris, S. L., Gioia, I., et al. 1990, ApJ, 348, 141

Stoughton, C., Lupton, R. H., Bernardi, M., et al. 2002, AJ, 123, 485

Strittmatter, P. A., Serkowski, K., Carswell, R., et al. 1972, ApJ, 175, L7

Swaters, R. A., Madore, B. F., & Trewhella, M. 2000, ApJ, 531, L107

Szomoru, D., Franx, M., & van Dokkum, P. G. 2012, ApJ, 749, 121

Tempel, E., Einasto, J., Einasto, M., Saar, E., & Tago, E. 2009, A&A, 495, 37

Tempel, E., Saar, E., Liivamägi, L. J., et al. 2011, A&A, 529, A53

Tully, R. B. & Fisher, J. R. 1977, A&A, 54, 661

Urry, C. M. & Padovani, P. 1995, PASP, 107, 803

Vega Beltrán, J. C., Pizzella, A., Corsini, E. M., et al. 2001, A&A, 374, 394

White, S. D. M. & Frenk, C. S. 1991, ApJ, 379, 52

White, S. D. M. & Rees, M. J. 1978, MNRAS, 183, 341

Williams, J. P., Blitz, L., & McKee, C. F. 2000, Protostars and Planets IV, 97

Wilson, A. S. & Colbert, E. J. M. 1995, ApJ, 438, 62

Wold, M., Lacy, M., Lilje, P. B., & Serjeant, S. 2000, MNRAS, 316, 267

Woltjer, L. 1990, in Active Galactic Nuclei, ed. R. D. Blandford, H. Netzer, L. Woltjer, T. J.-L. Courvoisier, & M. Mayor, 1–55

Wurtz, R., Stocke, J. T., Ellingson, E., & Yee, H. K. C. 1997, ApJ, 480, 547

Yee, H. K. C. & Green, R. F. 1984, ApJ, 280, 79

Yee, H. K. C. & López-Cruz, O. 1999, AJ, 117, 1985

York, D. G., Adelman, J., Anderson, Jr., J. E., et al. 2000, AJ, 120, 1579

Zel'dovich, Y. B. 1970, A&A, 5, 84

My contributions to the publications

Clustering environment of BL Lacertae object RGB 1745+398
Reduced and analysed the data. Main writer of the publication.

Environments of nearby quasars in Sloan Digital Sky Survey
Contributed in data analysis. Main writer of the publication.

Large scale environments of z<0.4 AGN
Analysed the data. Main writer of the publication.

Environments of galaxies in groups within the supercluster-void network
Analysed the data. Main writer of the publication.